Design of Carbon Nanotube Based Field Emission Facility

by

Yonghai Sun

A thesis

presented to the University of Waterloo

in fulfillment of the

thesis requirement for the degree of

Master of Applied Science

in

Systems Design Engineering

Waterloo, Ontario, Canada, 2008

Author’s Declaration

I hereby declare that I am the sole author of this thesis. This is a true copy of the thesis, including any required final revisions, as accepted by my examiners.

I understand that my thesis may be made electronically available to the public.

Abstract

The objective of this research is to build a prototype of a carbon nanotube (CNT)-based micro X-ray tube array, which can be used in a real-time cone-beam computed tomography (CT) scanner for cancer research. The X-ray tube array consists of an electron source, control grids, focusing electrodes, and an anode plate. All the experiments have been executed in an ultra high vacuum environment at a pressure of 10^{-7} Torr. A thin film consisting of multi-wall carbon nanotubes (MWNTs) was used as the electron source. A diode configuration was employed to test the field emission performance of the CNT thin film. The current density achieved was $1mA/cm^2$ at $10V/\mu m$. After the initial burn-in process, a relatively steady emission current was obtained for duration of 170 hours. The control grid was made of 25% opening space stainless steels mesh. Meshes with different wire diameters were tested in a triode structure, and some differences were observed. Multi-anode field emission tests and multi-tube electric field simulations were executed. Experiments and simulations have revealed crosstalk between pixels during field emission. Based on the above experiments and simulations, a signal pixel prototype has been fabricated and is being tested. Moreover, some potential optimizations that will be used in the second prototype are also discussed.

Acknowledgements

I would like to thank my supervisor, Dr. John T. W. Yeow, who has given me the opportunity to study medical devices that help people fight cancer.

I would also like to thank Dr. David A. Jaffray for his support, when I do my experiments in Princess Margaret Hospital, Toronto.

My partner labmates have also given me lots of help.

Finally, the support from my family is the most important impetus to my work.

Table of Contents

List of Figures

List of Tables

Chapter 1

Introduction

1.1 Motivation

X-ray was discovered more than one century ago, but the structure of an X-ray tube has not changed much since the first design. One of the most important components of an X-ray tube is the electron source. In traditional vacuum tubes, filaments were employed as a thermo electron emitter. The disadvantages of these hot cathodes are the long response time due to the thermionic cathodes and the high power consumption. Furthermore, the cathodes limit the lifetime of the tube due to mechanical wear. In addition, the thermionic electrons have random spatial distributions. As a result, fine focusing of the electron beam is very difficult [1].

An alternative mechanism to extract electrons is through field emission [2]. By this mechanism, the electrons near the Fermi level can tunnel through the energy barrier and escape to the vacuum under the influence of a sufficiently high external electric field. The physics of field emission from metallic surfaces is well understood [3]. Several advantages are associated with field emission cathodes, e.g., they have a faster response time, consume less power and have a longer lifetime.

Since the discovery of carbon nanotubes by Iijima in 1991 [4], extensive research on carbon nanotubes has been conducted. Field emission from carbon nanotubes was first reported in 1995 [5]. The remarkable field emission properties of carbon nanotubes are attributed to their

geometry, high thermal and electrical conductivity, and chemical stability. Field emission from carbon nanotubes has been studied extensively since it was discovered [6]. Due to the variety of carbon nanotubes, the properties of carbon nanotubes thin film are not understood thoroughly. It is still necessary to study the parameters of carbon nanotube thin film emitters to obtain the best performance.

1.2 Objectives

The main goal of this research is to design a real-time cone-beam CT scanner, which will be used to guide high energy radiation beams in cancer treatment [7, 8]. In radiation therapy, the precise treatment intent depends on the tumor type, location, and stage, as well as the general health of the patient. Radiation beams are commonly applied to tumors, but it is necessary to include a margin of normal tissue around the tumor to allow for uncertainties in daily set-up and internal tumor motion. To spare normal tissues, such as the skin or organs that radiation must pass through in order to treat tumors, shaped radiation beams are aimed from several angles to intersect at the tumor, providing a much larger absorbed dose there than in the surrounding healthy tissue [9]. With a real-time CT scanner, radiation oncologists can monitor the position and shape of tumors and adjust the treatment beams in vivo. The total radiation dose can be reduced as a result, which will benefit the patient by decreasing the margin of normal tissue exposed.

This study is focused on the first stage of a project to design the structure of a real-time cone-beam CT scanner and a micro X-ray tube, and to study the field emission properties of

carbon nanotubes. Suggested optimization methods will be included based on our experimental results.

1.3 Thesis Organization

The content of this thesis can be divided into three parts: (i) related concept and theory; (ii) experiment setup design and experiment results; and (iii) optimization methods and future works.

Chapter 2 focuses on the theory of field emission. The Fowler-Nordheim theory is the basic model of field emission. However, it cannot fully explain some phenomena, such as spike current and vacuum breakdown. As a result, the thesis briefly touches on the Nottingham effect and Joule heating as well as the possible reason for vacuum breakdown.

Chapter 3 gives some related properties of carbon nanotubes, for example, band structure and atom structure, the phenomena of field evaporation, and tip melting during field emission which have not been widely discussed in the literature.

Chapter 4 describes the experiment setup. The configuration of the system and the experiment circuit are explained, and the SEM images provided give a clear idea of the carbon nanotube thin films used in the experiments.

Chapter 5 presents the experiment results. The voltage-current curve is characteristic of that is yielded by the widely accepted Fowler-Nordheim theories. The long-term stability of these carbon nanotubes and the phenomena of vacuum breakdown and carbon nanotube degradation which have no established supporting theories, are also observed.

Chapter 6 discusses the factors of carbon nanotubes that affect field emission performance and possible methods to optimize it. These methods focus on the types of carbon nanotubes and the forms of the films.

Chapter 7 summarizes of this thesis and suggested plans for further experiments.

Chapter 2

Field emission

2.1 History of Field Emission

In 1897, R. W. Wood became the first person to describe the phenomenon of field emission [2], which he observed during experiments with a discharge tube. Initial theoretical insight into this process was provided by W. Schottky in 1923. He assumed that the electrons are emitted over a potential barrier at the surface lowered by the applied electric field [10].

In 1928, R.H. Fowler and L. W. Nordheim developed a theory of field emission based on quantum-mechanical tunneling of electrons through the surface potential barrier [3]. This theory accurately described the dependence of the emission current on the electric field and the work function, which is the energy needed to remove an electron from the Fermi energy level into a vacuum. It also followed from this theory that no external excitation is required for the initiation of this process. A clear evidence to this was obtained by J. E. Henderson et al [11] in their studies of the energy distribution of electrons and the measurements of the calorimetric effect.

An important development in the field emission area was the invention of the field emission microscope by E. W. Muller in 1936 [10]. The understanding of surface properties of field emission has benefited from this invention.

One of the most important results of the quantum-mechanical theory was the prediction of extremely high field emission current densities. In 1940, R. Haefer experimentally proved the feasibility of achieving high current densities of ~10^6A/cm ^{2}[10]. In 1950s, W. P. Dyke and his group achieved current densities of 10^7-10^8A/cm ^{2} under pulsed and steady-state conditions respectively [12, 13]. A number of important results were obtained by Dyke's group relate to the causes of instabilities and degradation of field emitters. It shows that the main cause of the emitter degradation was Joule heating of the tip by the emission current. M. I. Elinson and co-workers found that the maximum current values were dependent on the emitter geometry and showed that by increasing the tip cone angle, the current density could be increased by about an order of magnitude without emitter tip damage [10].

Further progress in research on field emission at extremely high current densities had been conducted by G. N. Fursey et al [10]. In DC experiments, thermal effects due to field emission at high current densities were demonstrated. A new type of instability caused by the spontaneous change of the cathode surface micro-geometry near the thermal destruction threshold was discovered. Current densities of 10^9A/cm ^{2} were observed with nanosecond range pulse lengths by G. A. Mesyats and G. N. Fursey [10]. Moreover, Current densities of ~10^{11}A/cm ^{2}were reported by G. N. Fursey et al, in 1998. These current densities are close to the theoretical supply limit of a metal's conduction band when the electron tunneling probability is unity [10].

Experimental and theoretical studies have been conducted to increase the stability of the field emission current and prevent ion bombardment of the cathode. Recent studies showed that an applied microwave field could reduce the intensity of cathode ion bombardment [10].

The practical applications of field emission began in 1959 by W. P. Dyke whose company produced pulsed X-ray apparatus for recording high-speed processes and compact X-ray sources for medicine [14]. Subsequently, a related phenomenon referred to as explosive emission was discovered [15]. In 1960s, the possibility of using field emitters as an electron sources for atomic-scale resolution electron microscope was demonstrated [16].

The research of using arrays of field emission cathodes in various microelectronic components and devices was suggested by K. R. Shoulders and initiated in the United States by C. A. Spindt [17]. The most striking example of the applications of field emission cathodes to an area of technological interest is in flat-panel displays.

In recent years, with the improvement of the experimental techniques, many new phenomena were observed, for example, broadening of the energy spectra at high current density [18], the presence of additional peak of energy spectra, and the presence of polarized electrons from metallic emitters coated with ferromagnetic films [10]. Although some of these phenomena cannot be explained by previous field emission theories, Fowler-Nordheim model is still the most widely used field emission theory.

2.2 Fowler-Nordheim Theory

The field emission process is a unique type of electron emission as it is exclusively due to quantum-mechanical effects. Field emission is the emission of electrons from the surface of a solid or liquid into a vacuum due to the presence of high electric fields. In the field emission process, electrons tunnel through the potential barrier at the surface, which the high electric field sufficiently narrows for the electrons to have a non-negligible tunneling probability.

Generally, the Fowler-Nordheim theory [19] is used to quantitatively describe the field emission process for metals. Quantifying the field emission process involves calculating the field emission current density as a function of the electric field. Since this process is essentially a tunneling process, both the tunneling transition probability for the electron to tunnel through the potential barrier and the number of electrons incident on the potential barrier must be found. Integrating these over all energy values gives the desired current density.

Figure 2-1 shows the potential barrier at the surface of a field emitter. Inside the metal, electrons occupy the energy band up to Fermi energy level. The potential energy outside of the metal is regarded as entirely due to the image forces $-e^2/4x$, where x is the distance from the surface of the metal. When an electric field is applied, the field contribution to the potential energy is $-eFx$, where F is the strength of electric field. Then, the effective barrier can be described by the potential function $U(x) = -\frac{e^2}{4x} - eFx$.

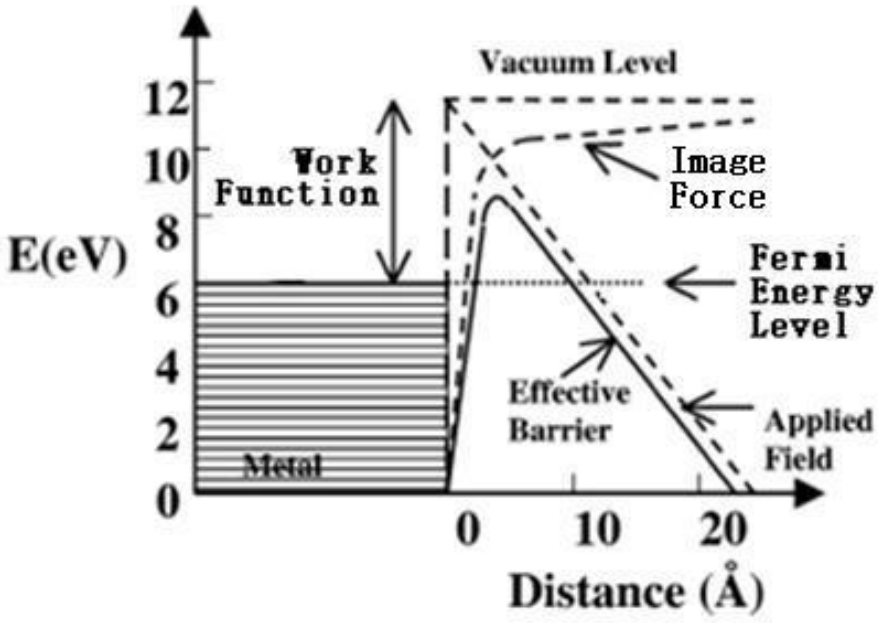

Figure 2-1: Potential Barrier of Field Emitter

The Fowler-Nordeim theory is based on the following main assumptions [10]:

1. *The metal obeys the free electron model of Sommerfeld with Fermi-Dirac Statistics.*
2. *The metal surface is planar, so the one-dimensional problem is considered. Thus as long as the potential barrier thickness is several orders of magnitude less than the emitter radius, this assumption is justified.*
3. *The potential within the metal is a constant; the applied electric field does not affect the electron states in the metal.*
4. *The calculation is performed for the temperature T=0 K.*

Under these assumptions, the current density is given by the equation:

$$j = e\int_0^\infty n(E_x)D(E_x, F)dE_x \qquad \textbf{(2-1)}$$

where e is the electron charge, $n(E_x)$ is the number of electrons per second having energies between E_x and $E_x + dE_x$ incident on 1 cm^2 of the barrier surface from within the metal, $E_x = p_x^2 / 2m$ is the part of the electron kinetic energy carried by the momentum component p_x normal to the surface, m is free electron rest mass, D is the barrier transparency and F is the applied electron field.

The barrier transparency is calculated using Wentzel-Kramers-Brillouin approximation [10]. For the potential barrier $U(x) = -\frac{e^2}{4x} - eFx$, which was described pervious, the transparency is given by [3, 10]

$$D(E_x, F) = \exp\left[-\frac{8\pi(2m)^{1/2}}{3he}\right]\frac{|E_x|^{3/2}}{F}\vartheta(y) \qquad \textbf{(2-2)}$$

where $\upsilon(y)$ is the Nordheim function

$$\vartheta(y) = 2^{-1/2}[1+(1-y^2)^{1/2}]^{1/2}\cdot[E(k)-\{1-(1-y^2)^{1/2}\}]K(k),$$

having for an argument

$$y = \frac{(e^3F)^{1/2}}{\varphi}$$

where φ is the work function, and

$$E(k)=\int_0^{\pi/2}\frac{d\alpha}{(1-k^2\sin^2\alpha)^{1/2}} \qquad K(k)=\int_0^{\pi/2}(1-k^2\sin^2\alpha)^{1/2}d\alpha$$

are complete elliptic integrals of the first and second kinds, with

$$k^2=\frac{2(1-y^2)^{1/2}}{1+(1-y^2)^{1/2}}.$$

Put the transparency equation (2.2) into the current density equation (2.1); then, the field emission current density at *T=0* follows the classic Fowler-Nordheim formula [3, 10]:

$$j=\frac{e^3}{8\pi h}\frac{F^2}{t^2(y)\varphi}\exp\left[-6.83\cdot10^7\frac{\varphi^{3/2}}{F}\upsilon(y)\right]$$

where $y=3.79\cdot10^{-4}\cdot\sqrt{F}/\varphi$ and $t(y)=\vartheta(y)-(2y/3)(d\vartheta(y)/dy)$.

The functions $\vartheta(y)$ and $t(y)$ have been tabulated by earlier researchers as can be found in [10] for instance.

This formula gives an excellent description of the exponential dependence of the emission current on work function φ and field strength *F*.

In the Fowler-Nordheim coordinates, the functional dependence $\ln j = f(1/U)$ is a straight line. Here, $I=j\cdot S$ is the emission current, with *S* as the emitting area and $F=\beta U$, where β is a geometric quotient determined by the geometry of the vacuum gap.

2.3 Thermal-field Emission

At nonzero temperatures, some electrons occupy energy levels higher than Fermi level. These electrons begin to contribute to the emission current. Emission of this sort is referred to as Thermal-Field emission. In this case, the general Fermi function should be used [10]:

$$f(E_x, T) = \frac{1}{\exp((E_x - E_F)/K_B T) + 1}$$

where E_F is the Fermi energy and K_B is the Boltzmann constant.

At T<1000K, an analytic expression can be obtained [20]. The ratio of $j(F,T)$ to that at zero temperature $j(F,0)$ may be expressed as

$$\frac{j(F,T)}{j(F,0)} = \frac{\pi\omega}{\sin \pi\omega}$$

where

$$\omega = \frac{4\pi\sqrt{2mk}\sqrt{\varphi}t(y)}{he}\frac{T}{F} \cong 9.22 \cdot 10^3 \sqrt{\varphi}\frac{T}{F}.$$

This expression holds as long as ω<0.7, such that $j(F,T)/j(F,0) < 5$. At high temperatures, when ω>0.7, the emission process moves into the regime of Schottky emission (Thermal-Field Emission) and higher temperatures will lead to the regime of pure thermionic emission.

2.4 Extending the Field Emission Theory

The model of the bulk metal and its surface in Flower-Nordheim theory is highly simplified. With the development of atomically sharp emitters used in tunneling spectroscopy, there came a need to understand the degree of localization of the tunneling process. However, there is no theory that permits accurate calculation of cathode operation characteristics. Some suggested solutions are listed below [10]:

1. Field Emission from Small-Scale Objects

   Many works show that one-dimensional approximation gives a fair description of the field emission process for atomically smooth emitters that have a radius greater than 0.1 μm. In this case, the width of the potential barrier is significantly less than the emitter's radius of curvature. On the other hand, with field emitters that have a radius of curvature close to or less than the barrier width, the assumptions of one-dimensional barrier and field uniformity over the apex of the tip are no longer justified. In particular, it is necessary to solve a three-dimensional Schrodinger equation using an asymmetric potential barrier and calculate the behavior of the potential near the surface, accounting for its radius and polar angle variations. As solving such a problem involves formidable difficulties, only rough calculations are made.

2. Effect of Fermi Surface Structure

The Flower-Nordheim theory is based on Sommerfeld's free electron model, and the Flower-Nordheim equation was derived using the Fermi-Dirac energy distribution function. Modern electronic theory of metals is based on the idea that electrons in metals behave as quasi-particles displaying a complex energy dispersion law. Theoretically, the temperature dependence of the field emission differs in principle from what is predicted by the free electron model. In this theory, the emission current decreases instead of increases as in the free electron model.

3. Many-Particle Effects

Fowler-Nordheim theory is essentially a one-electron theory. There are many phenomena that cannot be described in terms of the one-electron approximation. With the progress made in quantum-field methods due to statistical physics, it became possible to develop a multi-electron theory of field emission. Although there have been many attempts to apply this approach, the calculation of such a problem involves formidable difficulties. At present, the Fowler-Nordheim theory is still the most widely used field emission theory.

2.5 Maximum Field Emission Current Density

One of the most remarkable results of field emission quantum theory is the prediction of very high current density, which is possible due to two factors. First, if electrons exit the solid by a tunneling mechanism, no energy is required for maintaining the emission process. Second,

there is a very large reservoir of electrons near the Fermi level of a metal. As the density of the electrons in the conduction band is of the order of 10^{22}-10^{23} cm^{-3}, the theoretical limit of field emission current density is about 10^{11} A/cm^2 [10].

In a limiting case of a potential barrier transparency of 1, the maximum electron current density passing through a metal-vacuum interface can be expressed in the free electron model as

$$\vec{j} = e \iiint_{(\vec{p},\vec{n})>0} f(\vec{p})\vec{n} \cdot \frac{\vec{p},\vec{n}}{m} \cdot \frac{d^3\vec{p}}{h^3}$$

where, e and m are the electron charge and mass, respectively, $\vec{p}$ is the electron momentum, $\vec{n}$ is the unit vector normal to the emitting surface, and f is the Fermi function.

At $T = 0K$, $f(\vec{p})$ equals unity at the Fermi surface, and $f(\vec{p})$ outside it. For a spherical Fermi surface,

$$j = \frac{e}{m}\int_0^{2\pi} d\phi \int_0^{2\pi} d\theta \cdot \sin\theta \cdot \cos\theta \int_0^{pF} p^3 \frac{dp}{h^3}$$

where pF is the momentum of an electron at the Fermi surface. Integrating this equation, we can get a simple relation for the limiting emission current due to conduction band electrons in the metal:

$$j = \frac{\pi \cdot e m_e E_F^2}{h^3} \cong 4.3 \cdot 10^9 E_F^2 [A/cm^2]$$

where E_F is the Fermi energy (in eV) measured from the bottom of the conduction band. The field emission current density is usually lower than that predicted by this equation because of the onset of field emission instability at high current density.

2.6 Energy Spectra of Field Emission

The first attempt at measuring an energy distribution of field emitted electrons was made in 1931. Even though the resolution was very poor, this attempt did show that the electrons originated at the Fermi level as Fowler and Nordheim had predicted [21].

The potential distribution near the cathode surface (i.e., the potential barrier at the cathode micro-roughness) is written so:

$$\Phi(x) = \varphi_0 - e/(4x) - \beta U_0 x$$

where φ_0 is work function, U_0 is cathode surface electric intensity, e is electron charge, x is distance from the cathode, β is the field gain factor. As the potential distribution near the micro-roughness is essentially nonlinear, the equation should be written as

$$\Phi(x) = \varphi_0 - e/(4x) - T(x)$$

where $T(x)$ is a nonlinear function generally depending on the shape of the micro-roughness. Every shape of the micro-roughness has its own form of the function $T(x)$. The barrier structure and field emission current density and energy spectrum are significantly determined by the dimensionless parameters $M = \varphi_0 / U_0 a$, where a is the micro-roughness height [22].

In a number of papers, the possibility of groups of electrons tunneling into a vacuum, correlated in space and time, has been discussed. The first direct measurement of statistical field emission events was reported in 1965. A complete investigation of the statistics of field emission from tungsten shows that its spectra have a single peak. In G. Fursey's experiment, many-particle effects were not observed. This result infers that the multi-peak spectra observed in other's experiments are connected with parasitic secondary emission from intermediate electrodes. In measurements carried out with an intermediate accelerating electrode, a secondary emission multi-peak spectrum was obtained. Later, a detailed investigation of the field emission statistics for different metals was conducted. The results show with a likelihood of 99.9% accuracy that the field emission from certain metals is a single particle.

2.7 Heating in Field Emission

For many years, it was believed that the major cause of emitter destruction was Joule heating. However, some experiments indicate that the dominant contribution to the thermal balance during field emission is due to Nottingham effect, which is a purely quantum-mechanical energy exchange process. According to this theory, most of the electrons that tunnel through the potential barrier are at lower energy levels than the Fermi level. After these electrons have been emitted into the vacuum, electrons in the conduction band will replace them. As the electrons in the conduction band have higher energy than that of the emitted electrons, they transfer energy to the lattice when replacing the emitted electrons. At a high current

density, the energy associated with the Nottingham effect could exceed the energy due to Joule dissipation. Together with Joule heating, Nottingham heating causes a rapid temperature rise in the emitter. After the emitter is heated to a high temperature, most of the emitted electrons are at a higher energy level than the Fermi level; the Nottingham effect begins to cool the cathode. This specific temperature is referred to as the inversion temperature [23]. Joule heating and Nottingham effect together can heat the cathode faster than each of can alone.

The first theoretical analysis of emitter tip self-heating was carried out by W. Dolan et al [12]. They calculated the value of the steady-state maximum current density for a one-dimensional model of an emitter tip. The three-dimensional problem was solved by Glasanov, Baskin, and Fursey using calculations conducted for a tip of the form suggested by Dyke [10]. These calculations took into account Joule heating, Nottingham and Thomson effects, and thermal radiation [24]. The temperature dependence of the resistivity, heat capacity, and surface emissivity were tabulated. The most important result of these calculations is their description of the overheated core's formation inside the emitter apex. The temperature at the surface may be well below the melting point, while in the internal region, it may be equal to several tens of thousands of degrees, leading to enormous temperature gradients and the generation of large thermoelastic stresses. The value of tangential stresses at the tip surface can exceed $2 \cdot 10^9$ Pa [25], which can destroy the tip before the melting point is reached.

It is known that the maximum attainable field emission current density is limited by Joule Heating of the lattice and Nottingham effect. Whereas Joule Heat is released throughout the bulk of the cathode, the heat produced by Nottingham effect is localized to the near surface region whose thickness is of the order of an electron-phonon free path. Above the Debye temperature, the Nottingham effect is a surface phenomenon. Lowering the emitter temperature causes a significant reduction in Joule heating and a considerable increase in the electron-phonon free path, which shifts Nottingham heating to a bulk effect. Therefore, the maximum field emission current density can be increased by decreasing the emitter temperature [26].

2.8 Field Emission and Vacuum Breakdown

Vacuum breakdown is a complicated phenomenon connected with a large amount of processes in strong electric fields. It is now firmly established that field emission plays an important role in breakdown initiation [27]. In many cases, vacuum breakdown is initiated by the thermal explosion of a micro-tip at the cathode surface, caused by the field emission current. Emitters heated by field emission currents result in thermal instability and transition from field emission to explosive emission and vacuum breakdown [15, 28].

Sometimes breakdown is preceded by the appearance of micro-discharges, low-power pulses of pre-breakdown current, and peak current. The repetition rate of micro-discharges increases with applied voltage. With mass spectrometry, it has been established that micro-discharge currents contain not only an electronic component, but also positive and negative ions [29].

One of the most comprehensive studies in which the DC breakdown mechanism has been confirmed experimentally is that performed by D. Alpert and co-workers [30]. They showed that, taking into account the factor of electron field enhancement at micro-protrusions, local breakdown electric field appears to be independent of gap spacing and is unaffected by electrode geometry. The additional observation that the electric field at which vacuum breakdown takes place is a constant can be interpreted so that breakdown occurs as the density of the field emission current from cathode micro-protrusions reaches a certain value [29, 31].

When a high voltage is applied to a gap for a long time, a variety of processes occur at the electrode and in the gap. It is desirable to identify the processes directly responsible for the initiation of breakdown and domination of the mechanism. In practice, some pre-breakdown processes are either undetectable or they cannot be identified and resolved in space and time.

In numerous experiments, it has been established that breakdown voltage depends to a large measure on electrode material. There is a tendency for the breakdown voltage to increase as the melting temperature and mechanical strength of the electrode material increase. The breakdown voltage is strongly affected by the duration that the voltage is applied and the rate at which voltage is increased. Other factors are also known to influence breakdown voltage, namely, the conditioning of the gap by successive breakdowns, the vacuum conditions, the parameters of the electric circuit in which the gap is connected, the electrode curvature, area and temperature, etc. [28, 29].

Chapter 3

Introduction of Carbon Nanotubes

3.1 Physics of Carbon Nanotubes

Carbon Nanotubes were discovered and first characterized in 1991 by Iijima [4] of NEC laboratories. Shortly after the discovery of multiwall carbon nanotubes, single wall carbon nanotubes were synthesized [32].

Because the microscopic structure of single wall carbon nanotubes is closely related to that of graphene, the tubes are usually labeled in terms of the graphene lattice vectors. This structure can be specified by its circumferential vector, as defined by the chiral vector that connects two crystallographically equivalent sites on a graphene sheet. In this way, a single wall carbon nanotube's geometry is completely specified by a pair of integers (n,m) denoting the relative position of the pair of atoms on a graphene strip. When rolled onto each other, these atoms form a tube. In such a tube, *a1* and *a2* are the unit vectors of the hexagonal honeycomb lattice [33, 34].

Due to periodic boundary conditions along the circumferential direction of the tube, the allowed wave vectors "around" the nanotube circumference are quantized: they can take only a set of discrete values. In contrast, the wave vectors along the nanotube axis remain continuous for infinite tubes. Plotting these allowed vectors for a given nanotube onto the Brillouin zone of graphene generates a series of parallel lines. The length, number, and orientation of these cutting lines depend on the chiral indices (n,m) of the nanotube. The

basic idea behind the zone-folding approximation is that the electronic band structure of a specific nanotube is given by superposition of the graphene electronic energy bands along the corresponding allowed *k* lines [35, 36].

Figure 3-1 [36] shows the graphene honeycomb network with lattice vectors a1 and a2. The chiral vector Ch=5a1+3a2 represents a possible wrapping of the two-dimensional graphene sheet into a tubular form. The direction perpendicular to $\overrightarrow{C_h}$ is the tube axis. The chiral angle is defined by the $\overrightarrow{C_h}$ vector and the $\overrightarrow{a_1}$ zigzag direction of the graphene lattice. Figure 3-1 represents a (5,3) nanotube under construction, with the resulting tube is illustrated on the right.

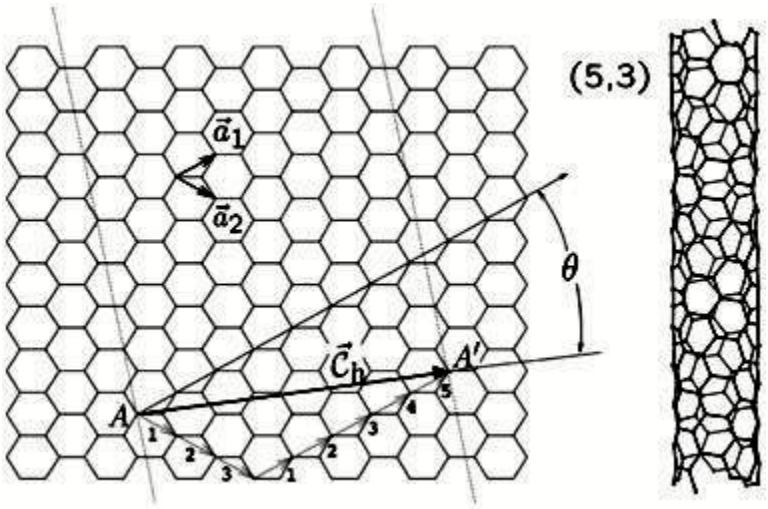

Figure 3-1: Graphene Honeycomb Network

Carbon nanotubes have unique electronic properties due to electron confinement in the same direction to the axis of the tube as carbon nanotubes consist of a monolayer of graphene

sheet. Since their discovery, carbon nanotubes have been regarded as potential molecular quantum wires. Their electrical conductivity is about 6 orders of magnitude higher than copper [37]. Depending on the details of their atomic arrangement, they behave as metals or semiconductors. All (n,n) tubes (armchair type) are metallic, while (n,m) ($n \neq m$) tubes are semiconductors. If 2n+m or n+2m are multiples of 3, then it is a narrow-gap semiconductor, otherwise it is wide-gap semiconductor. In multi-wall nanotubes, the electrical properties of individual tubes vary greatly from tube to tube mainly because of disorder and localization effects. Figure 3-2 shows the atomic structures of (12, 0) zigzag, (6, 6) armchair, and (6, 4) chiral carbon nanotubes [36].

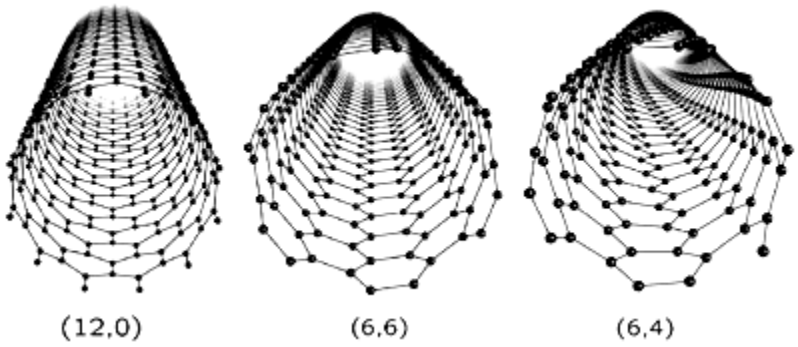

Figure 3-2: Atomic Structures of Carbon Nanotubes

Carbon nanotubes have some unique mechanical and electrical properties. As the C=C bond is considered to be the strongest bond in nature, carbon nanotubes have great strength in the direction of the nanotube axis and thus have a very high elastic modulus. Young's modulus is of the order of 1 TPa [38], in contrast to, for example, the 70 GPa of aluminum. Carbon nanotubes also have high thermal conductivity in their axial direction [39]. It is estimated to

be about five times that of the copper. In the case of single-wall carbon nanotubes at low temperature, the electronic waves may remain extended along the nanotube over several microns, which shows that the motion of electrons are quantum mechanical in nature.

3.2 Bands Structure of Carbon Nanotube

As the nanotubes are one dimensional, their Brillouin zone is one dimensional as well. The nanotube band structure is therefore represented along the ΓX direction [36].

In (5,5) armchair nanotubes, six bands for the conduction and an equal number for the valence states are observable. However, four of these bands are degenerate, leading to ten electronic levels in each case, consistent with the ten hexagons around the circumference of the (5,5) nanotube. The energy bands of all armchair nanotubes exhibit a large degeneracy at their zone boundaries because of the absence of dispersion along the segments connecting the neighboring centers of the BZ sides, an effect that yields the so-called trigonal warping of the bands [40].

The 1D dispersion relations E(k) for the (9,0) and (10,0) zigzag nanotubes are illustrated in Figure 3-3. As expected, the (9,0) tube is metallic, with the Fermi surface located at Γ, whereas the (10,0) nanotube exhibits a finite energy gap at Γ. In particular, in the case of the (10,0) nanotube, there is a dispersionless energy band at $E/\gamma_0 = \pm 1$, which gives a singularity in the density of states at these particular energies. For a general (n,0) zigzag nanotube, when n is a multiple of 3, the energy gap at k=0 (Γ point) becomes zero. However, when n is not a multiple of 3, an energy gap opens at Γ. The corresponding densities of states

have a zero value at the Fermi energy level for the semiconducting nanotube and a small nonzero value for the metallic one.

The band structure and density of states for different kinds of nanotubes within the zone-folding model are showed in Figure 3-3 [36]. In these figures, the Fermi level is located at zero energy. The corresponding figures are (a) a (5,5) armchair nanotube, (b) a (10,0) zigzag nanotube, (c) a (9,0) zigzag nanotube, and (d) a (8,2) chiral nanotube.

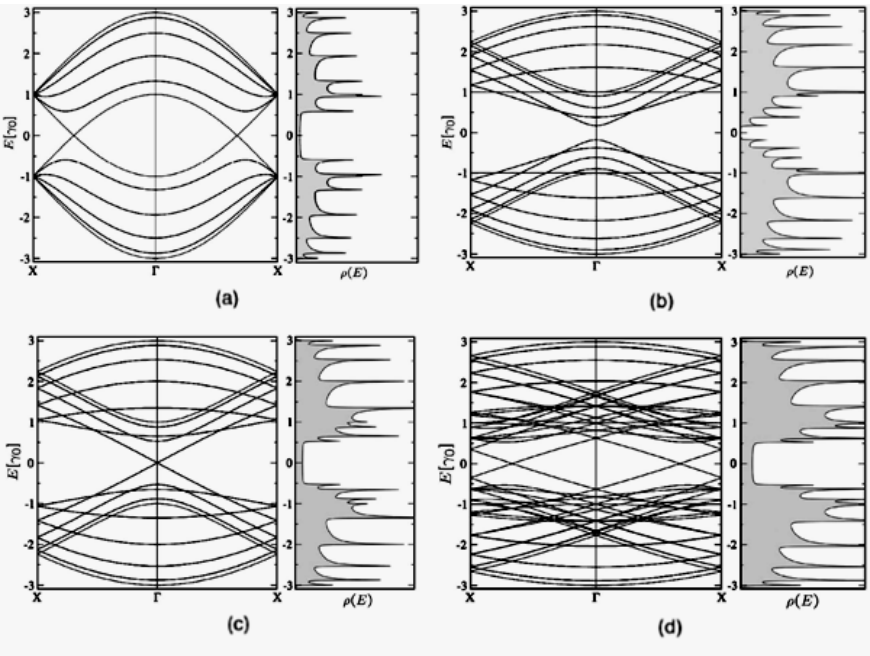

Figure 3-3: Band Structure and Density of States for Nanotubes

In semiconducting zigzag or chiral nanotubes, the band gap is independent of the chiral angle and varies inversely with the nanotube diameter. Density-of-states measurements by scanning tunneling spectroscopy provide a powerful tool for probing the electronic structure

of carbon nanotubes. It can be shown, indeed, that under some assumptions, the voltage-current derivative dI/dV is proportional to the density of states [41].

The density of states $\Delta N/\Delta E$ represents the number of available states, ΔN, for a given energy interval, ΔE ($\Delta E \rightarrow 0$). This density of states is a quantity that can be measured experimentally under some approximations. The shape of the density of states is known to depend dramatically on dimensionality. In 1D, the density of states diverges as the inverse of the square root of the energy close to band the extremes. These "spikes" in the density of states are called Van Hove singularities and manifest the confinement properties in directions perpendicular to the tube axis. As carbon nanotubes are one dimensional, their corresponding density of states exhibit such spiky behavior at energies close to band edges. The position of these Van Hove singularities can be analytically derived from the dispersion relations [36].

3.3 Defect and Emission Sites of Carbon Nanotubes

As with any material, the existence of defects in carbon nanotubes affects those tubes' material properties. Defects can occur in the form of atomic vacancies. A high density level of such defects can lower the tensile strength of a carbon nanotube by up to 85%. Another form of defect is known as the Stone Wales defect, which creates a pentagon and heptagon pair by rearrangement of the bonds. Because of the very small structure of CNTs, their tensile strength is dependent on their weakest segment in a similar manner to a chain, where a defect in a single link diminishes the strength of the entire chain [42].

The carbon nanotubes' electrical properties are also affected by the presence of defects [43], which often results is lowered conductivity through the defective region of the tube. Some defect forms in armchair-type tubes (which can conduct electricity) can cause the region surrounding a defect become semiconductor. Furthermore, single monoatomic vacancies induce magnetic properties.

The carbon nanotube's thermal properties are heavily affected by defects [44]. Such defects lead to phonon scattering, which, in turn, increases the relaxation rate of the phonons. This increase reduces the mean free path and reduces the thermal conductivity of nanotube structures.

The stability of the emission current is important for field emission devices. However, it has been reported that either the current becomes highly unstable or that structural damage of carbon nanotubes occurs when the current or electric field is high. With respect to the stability of the emission current, structural change at the tip of the carbon nanotube is an important subject in understanding the mechanism of the current fluctuation. Though it is expected that the emission sites are closely related to the form of the tips of the carbon nanotubes, the relation between the emission sites and the tip forms is not clear [45]. The emission sites of carbon nanotube can be observed using field emission microscope and field ion microscope [46]. T. Fujieda et al. observed a bright spot at the tip of a multi-wall carbon nanotube during their field emission experiments [47]. The bright spot was assumed to be related to the emission site on the multi-wall carbon nanotube. They also reported structural changes to the tip, namely, the outer layers of multi-wall carbon nanotubes were peeled off

during field emission, and then functioned as second emission sites for the concentration of the electric field. Y. Saito et al. observed the tip of carbon nanotubes with field emission microscope [48] and reported that capped multiwall carbon nanotubes gave field emission patterns consisting of a number of bright solid spots. For open carbon nanotubes, annular bright rings were observed.

The ends of capped carbon nanotubes are capped with curved graphene layers. At least 12 pentagons are needed to close the hexagonal network of a nanotube [49]. Figure 3-4 [50] shows some possible tip structures for carbon nanotubes. In these structures, pentagons are included, and the shape of the cones changes as a function of the number of pentagons. A pentagon introduces a positives curvature to a hexagonal lattice, and the strain is localized around the pentagon. Regions other than pentagons are flat, so the portions where pentagons are located extrudes. Since the electric field concentrates on sharp points, the portions where pentagons located are the most probable emission site.

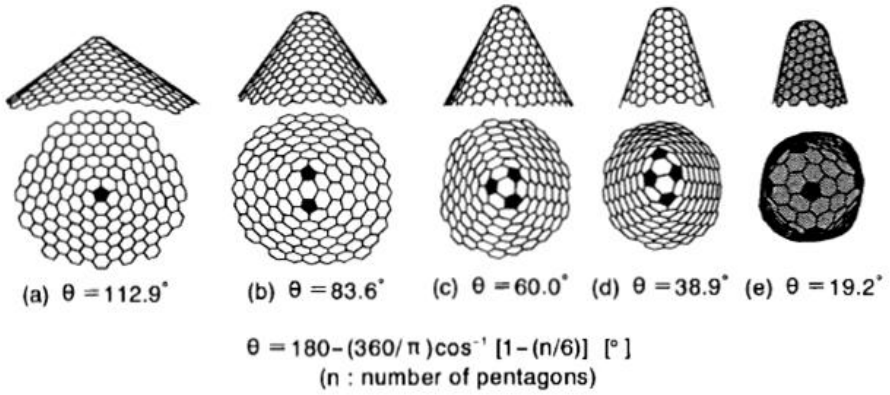

Figure 3-4: The Possible Tip Structure with Cone Shape

3.4 Energy Spectra of Emitted Electrons

One important advantage of field emitters is that the energy spread of them is far lower than that of thermo emitters [11, 49]. Electron energy analyzers are used to measure the energy distributions of emitted electrons. The full width at half maximum of the distribution is typically 0.45 eV for a metal. Many studies show that the field emission energy distribution of nanotubes is significantly narrower than that for a metallic emitter. Figure 3-5 shows one of the field electron energy spectrums obtained on a multi-wall carbon nanotube film by Bonard et al [51]. In their measurement, the full width at half maximum is less than 0.2cV.

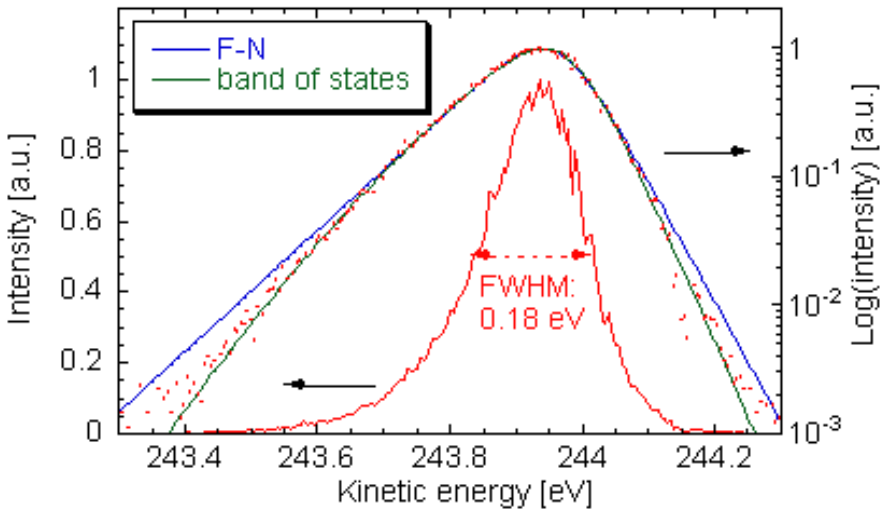

Figure 3-5: Field Emission Electron Energy Spectrum

C. Oshima et al. reported that the shape of the main peak in the spectrum of carbon nanotubes is clearly different than that seen in normal tungsten tip emitters [52]. The energy spectra peak of carbon nanotubes is broader than those of a tungsten emitter. The broad peak

of carbon nanotubes show that the high-energy electrons are injected into the end cap from the tube interior, and band bending occurs near the emission sites.

3.5 Work Function of Carbon Nanotube

The material's work function is an important parameter of field emitters. The sidewall and the tip of carbon nanotubes have different work functions. The applications of nano-electronics focus on the work function of the sidewall [53]. In field emission applications, the work function of tips and defects are the point of interest because of their emission of electrons [52]. Many methods have been developed based on different physical effects to measure and calculate work function. These methods are divided into two groups: one is to measure the energy of photons emitted or absorbed; the other one is to measure the contact potential difference between the sample and a reference electrode.

Methods based on photoemission and thermionic emissions are generally used to measure the work function of carbon nanotubes. It was reported that the work functions of single-wall and multi-wall carbon nanotubes are between 4.7 and 5.1 eV [53-56]. However, with these methods, we can obtain only the work function of the sidewalls.

Energy distribution measurement is the only method to determine the work function of a field emitter. Many experiments have been conducted to measure the work function of carbon nanotubes, but the results are still fragmentary [35]. Most of the reported work functions of nanotubes are around 5eV, which is the value of the work function of carbon.

Chapter 4

Experiment Setup

4.1 Overview

Figure 4-1 shows the whole setup of our experiments. The system was composed of four major sub-systems, i.e., (i) the field emission configuration which is mounted inside the vacuum chamber, (ii) the data acquisition and control circuit, (iii) the vacuum pump and vacuum chamber, (iv) a high voltage power supply.

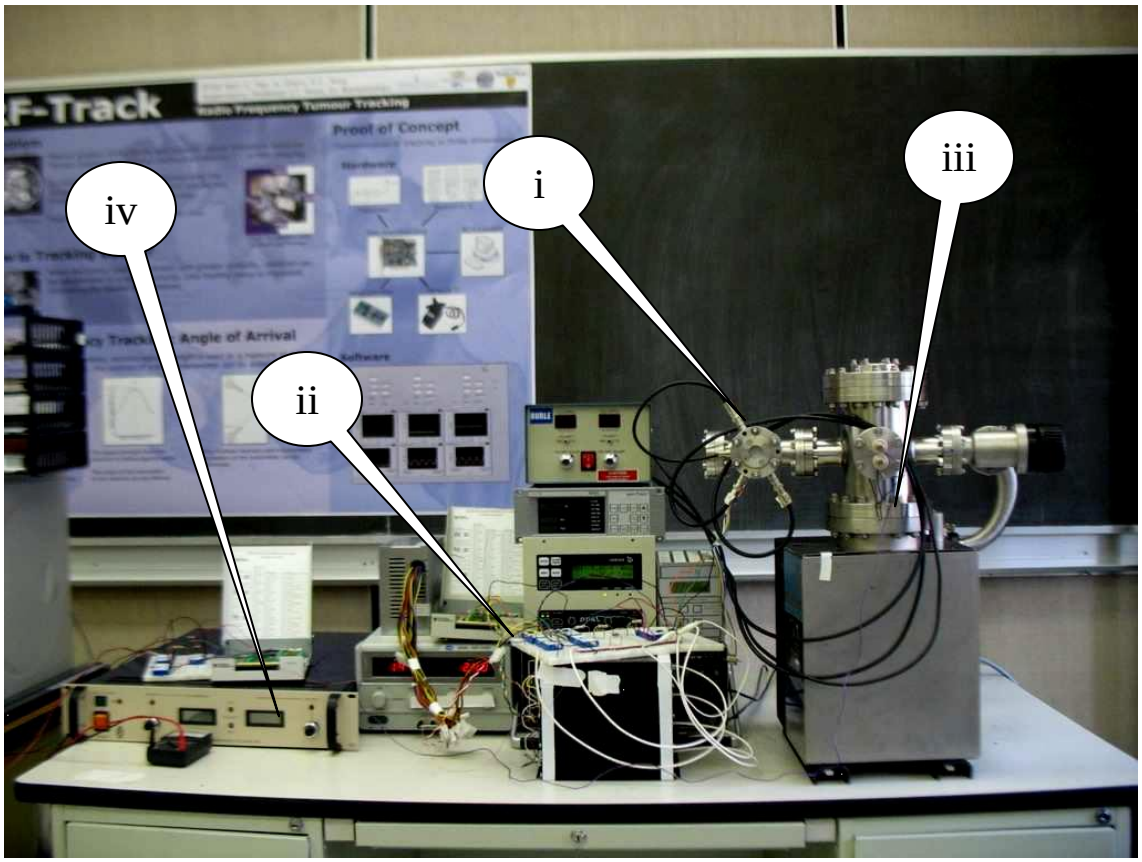

Figure 4-1: Experiment Setup

Successful field emission production can occur only in an ultra-high vacuum (UHV) condition where the emitted electrons can actually reach the anode and avoid colliding with air particles [6]. Therefore, a vacuum chamber had to be designed to house the cathode and the anode in a vacuum environment.

The behavior of its cathode is key to obtaining a high performance field emission device. The performance of different kinds of field emission cathodes, such as metallic Spindt-type emitters [57] and nano-structured diamonds [58], has been studied for a long time. However, Spindt-type emitters suffer from a high manufacturing cost and limited lifetime. Their failures are often caused by ion bombardment from residual gas species that blunt the emitter cones. On the other hand, nano-structured diamonds are unstable at high current densities. Carbon nanotubes, an allotrope of carbon, have the potential of being used as cathode material in field emission devices.

4.2 Carbon Nanotubes Film

The multi-wall carbon nanotube films used for this study were realized by plasma-enhanced hot filament chemical vapor deposition (PECVD) at NanoLab Inc. Acetylene (C_2H_2) gas was used as the carbon source for the growth of carbon nanotubes, and ammonia (NH_3) gas was used as both a catalyst and as a dilution gas. In this process, the intensity of plasma was found to be critical in determining the aspect ratios of CNTs and their range of both site and height distributions within a given film. As the plasma intensity was increased, two structural

changes were observed: (i) a decrease in average tube diameters and (ii) a significant increase in tube lengths.

Three kinds of multi-wall carbon nanotube films were used in these experiments. The specifics of the carbon nanotube thin films are listed in Table 4-1. Film 1 has the highest density we were able to obtain from Nano-Lab, and the density of Film 2 and 3 is the theoretical optimized density for field emission. The method of calculating the optimized density is described in Chapter 6. The length and diameter of the carbon nanotubes listed below were measured after the films were fabricated because these values cannot be controlled accurately during the process of fabrication

	Film 1	Film2	Film 3
Substrate	Cr-Cu	Cr-Stainless Steel	Cr-Quartz
Density(cm^{-2})	1×10^{9}	$5\text{-}10\times10^{6}$	3.5×10^{6}
Length(μm)	10	13	15
Diameter(nm)	100	50	150
Shape of Film	Round	Square	Square
Area	10 mm diameter	8mm×8mm	8mm×8mm

Table 4-1: Film Specifics

In most of our experiments, films with a Cu-Cr substrate and the highest density were employed. The current-voltage characteristics and long-term stability experiment results of these films are described in the next chapter. The influence of substrate materials on field emission and multi-anode crosstalk is also analyzed. The SEM images of carbon nanotube films with different densities are shown in the Figure 4-2 and 4-3.

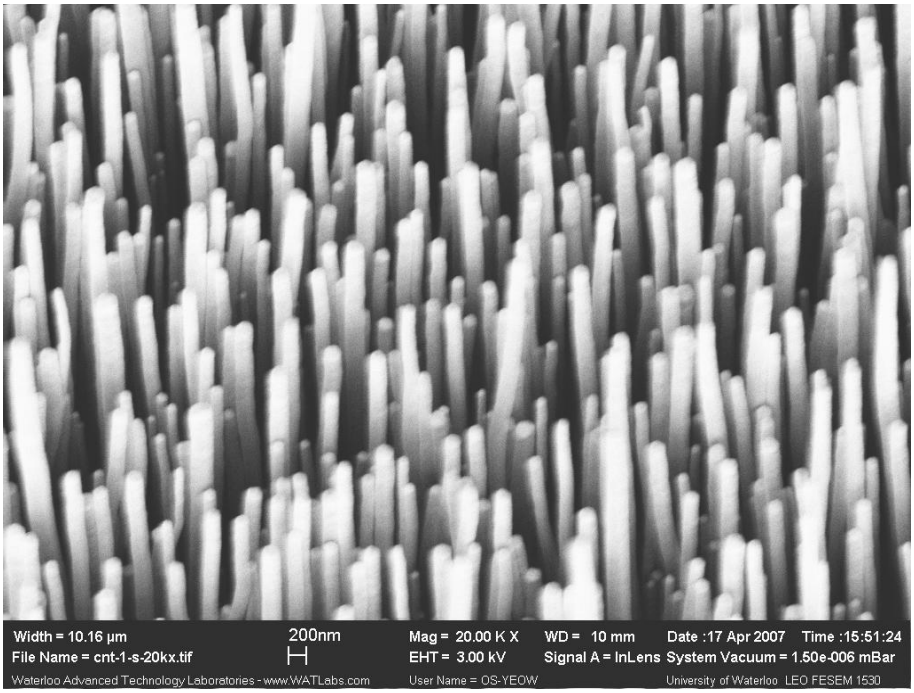

Figure 4-2: SEM Image of High Density Carbon Nanotube Film

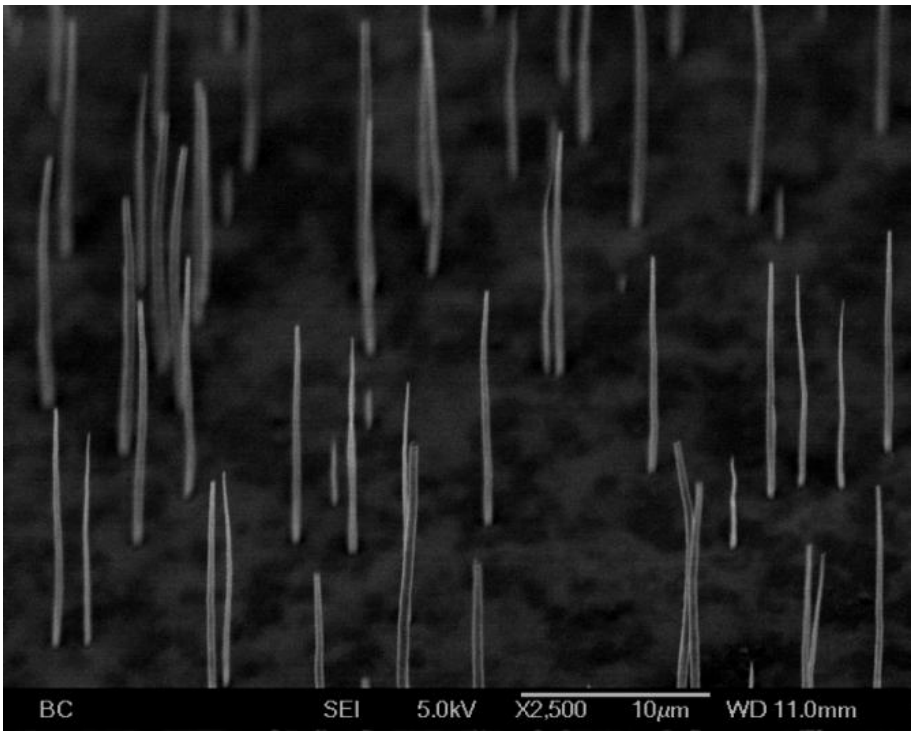

Figure 4-3: SEM Image of Low Density Carbon Nanotube Film

4.3 Diode Structure Configuration

A diode structure configuration consists of three parts: (i) anode; (ii) spacer; and (iii) cathode. The anode is a flat metal plate, which is made of either copper or aluminum. The spacer is made of dielectical materials. PVC, acrylic, and Teflon were tested in our experiments. The best material is Teflon, because it has very low outgassing and excellent dielectric properties. The cathode is an aligned carbon nanotube thin film grown on a flat substrate. The substrate is coated with a thin layer of chromium, and the carbon nanotubes grown on the chromium layer. Copper, stainless steel, and quartz are used as substrates in our experiments separately,

but most of the experiments are conducted on carbon nanotube thin films with a copper substrate.

In our experiments, the first challenge is to find a method to measure the distance between the anode and the carbon nanotubes. There are many methods to measure the gap, but each one has its limitations.

At the very beginning, a micrometer was used to adjust the gap. The resistance between the cathode and anode is measured and used to identify the touch point. The readout of the micrometer at the touch point is set as reference zero. Then, the gap was determined by the movement of the micrometer. This method has some big disadvantages. First, when the anode “touches” the cathode film, the carbon nanotubes may be damaged. Second, the film is not perfectly flat; thus, the highest point of the film will determine the touch point, thereby affecting the accuracy of the measurement.

Another method is to measure the capacitance of the structure and to calculate the gap with the parallel plate capacitor equation. This calculation is based on an assumption that the carbon nanotube film can be viewed as a flat plate. Compared to the first method, this method is more accurate but more complex. The problem of this method is that the performance of the micrometer affects measurement results. When the thimble is turned, the rod moves not only back and forth, but also perpendicular to the rods, which changes the constant gap distance between the electrodes and affects accuracy.

Spacers are the most commonly used component to determine the gap. The thickness of the spacer is the distance between the anode and the substrate. The problem of this method is that the actual distance between the carbon nanotube tips and the anode is still unknown because the length of the carbon nanotubes is not accurate. Compared to other methods, this is the easiest way to control the gap. Figure 4-4 shows the diode structure, where aluminum plate was used as the anode, and PVC thin film was used as the spacer.

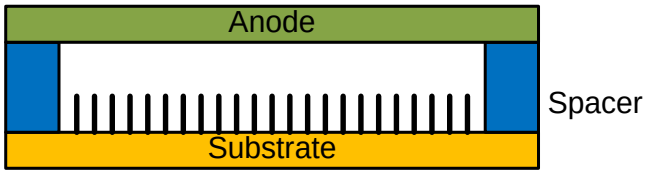

Figure 4-4: Configuration of Diode Structure

The main problem of this diode structure was that, during the field emission experiments, some of the nanotubes were peeled off from the substrate, and then accumulated along the spacers, making a conducting path between the anode and the cathode, and causing a short circuit. To solve this problem, an improved diode structure is employed.

In the improved diode structure, the distance between the nanotubes and the spacer and the gap between the anode and cathode were increased. This increase effectually avoided the accumulation of carbon particles between the cathode and anode. In this structure, some conductive adhesives were used to fix the substrate onto the holder. The thickness of the adhesive layer is not uniform, so the distance of the film and anode has a measurement error. This error affects the calculation result of the field emission property but will not affect the

system structure's designation. Figure 4-5 shows the improved diode structure, where the anode and the cathode holder are made of a copper plate, and the spacer is made of a Teflon tube.

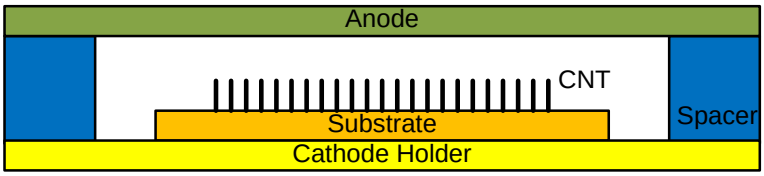

Figure 4-5: Configuration of improved Diode Structure

4.4 Triode Structure Configuration

The final structure of a carbon nanotubes based X-ray tube is a triode configuration. A gate electrode is used to attract electrons from the cathode, and the anode is used to accelerate the emitted electrons. The purpose of using a gate electrode is to achieve a relatively low control voltage. Figure 4-6 shows the structure of a triode setup. In this setup, the target and cathode holder were made of a copper plate; the gate electrode was a stainless steel mesh, and the spacers were made of a Teflon tube. Meshes with different density were tested to find out the best ratio of the anode current to the total emitted current. In these tests, only stainless steel woven wire meshes were used. Figure 4-7 shows a microscope picture of a 50X50 mesh. In these meshes the diameter of the wire is equal to the distance between the wires, so the opening space of the mesh is about 25%. Since different meshes have different wire diameters, the thickness of the mesh varies. Furthermore, the surface of the mesh is not flat at

all, so the width of the gap cannot be determined accurately. In a rough test, over 40% of electrons passed through the mesh.

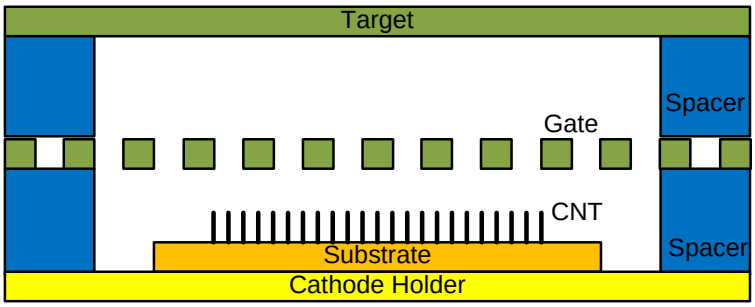

Figure 4-6: Configuration of Triode Structure

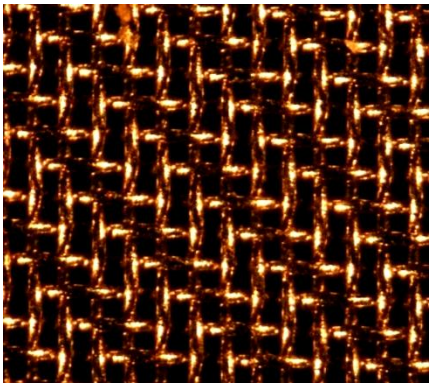

Figure 4-7: Stainless Woven Wire Steel Mesh

4.5 Experiment Circuit

Figure 4-8 shows an abridged general view of the experiment circuit for one testing channel. The most important component of this circuit is the wide bandwidth, 3-port high voltage isolation amplifier, which provides high accuracy and complete galvanic isolation with both signal and power path. In the experiments, all the data were collected by a data acquisition

card: i.e., voltage, current, and pressure in the vacuum chamber. Because both the ion vacuum pump and high voltage power supply were based on switched-mode power supply, they produced a lot of high frequency noise, which imported a significant systematic error into the data acquisition card and affected the accuracy of the test results. The frequency of these noises is about 150 kHz, which is much higher than the maximum working frequency of the isolation amplifier, so the noises could not pass through the amplifier. In this case, the amplifier not only isolated the date acquisition card from high voltage, but also filtered the high frequency noises.

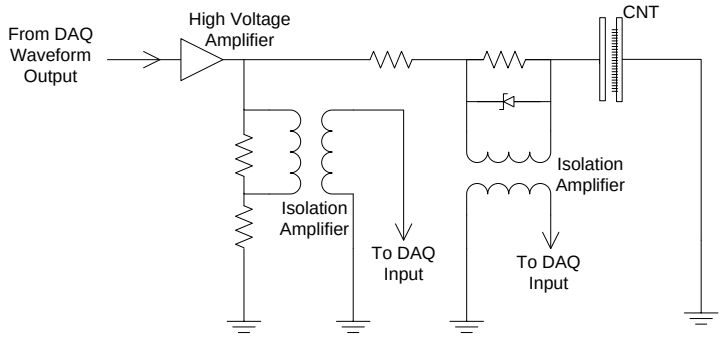

Figure 4-8: Experimental Circuit

4.6 Outgassing and Dielectric in Vacuum

Outgassing is the slow release of a gas that has been adsorbed in some material. It is a challenge in the creation and maintenance of clean, high-vacuum environments. The rate of outgassing increases at higher temperatures because the vapor pressure and rate of chemical reaction increases. For most solid materials, the methods of manufacture and preparation can

reduce the level of outgassing significantly. Cleaning surfaces or baking individual components or the entire assembly before use can drive off volatiles.

NASA maintains a list of low-outgassing materials to be used for spacecraft. The outgassing data can be presented in many ways, but the most commonly used are Total Mass Loss (TML) and Collected Volatile Condensable Materials (CVCM). The criteria of outgassing for NASA are maximum Total Mass Loss (TML) of 1.0 percent and maximum Collected Volatile Condensable Material (CVCM) of 0.10 percent. Table 4-2 [59] lists the Total Mass Loss and Collected Volatile Condensable Material of the materials used in our experiments. These materials have very low outgassing, and they perform well in our experiment.

Material	TML(%)	CVCM(%)
Stainless Steel	0.02	0.00
Glass	0.06	0.00
Copper	0.17	0.00
Aluminum	0.02	0.00
Teflon	0.02	0.01

Table 4-2: Outgassing of Materials

In our design, a 40 kV high voltage is applied to the silver target; the distance between the target and other parts is very small, so the dielectric strength of the isolating material is a very important parameter. Compared to other materials with high dielectric strength, e.g.,

glass and mica, Teflon is much easier to machine, so Teflon is chosen as the dielectric material in the prototype fabrication.

Chapter 5

Field Emission Experiment Result

5.1 Current-Voltage Characteristic

The experiments were conducted in an ultra-high vacuum environment. A high voltage power supply was connected to the anode, and the carbon nanotube film cathode was grounded. The current and the voltage were measured using a data acquisition card. The output voltage of the power supply was controlled by a computer through the data acquisition card.

Varied configurations of diode structure were used to test the voltage-current characteristic. Different gap distances and voltage waveforms were used in the experiments. Figure 5-1 shows one of the current-voltage curves. In this experiment, the gap is about 150 micrometer; the voltage of the anode increases from 0V to 1800V within 20 seconds. There are two regions of operation. At low forward bias, there is no forward current. The forward current becomes appreciable as the bias voltage is increased above a turn-on voltage.

Two parameters are chosen to evaluate the field emission performance of the carbon nanotubes films: the emission current density and the threshold field, (a point at which an emission current density of 10 $\mu A/cm^2$ is drawn). In this experiment, the area of the emitter is $0.785cm^2$, and the gap is about $150\mu m$, the corresponding threshold is $7.3V/\mu m$. Figure 5-2 shows the Fowler-Nordheim curve of the experiment described above. The curve fits to a straight trend line over a wide range of emission current values.

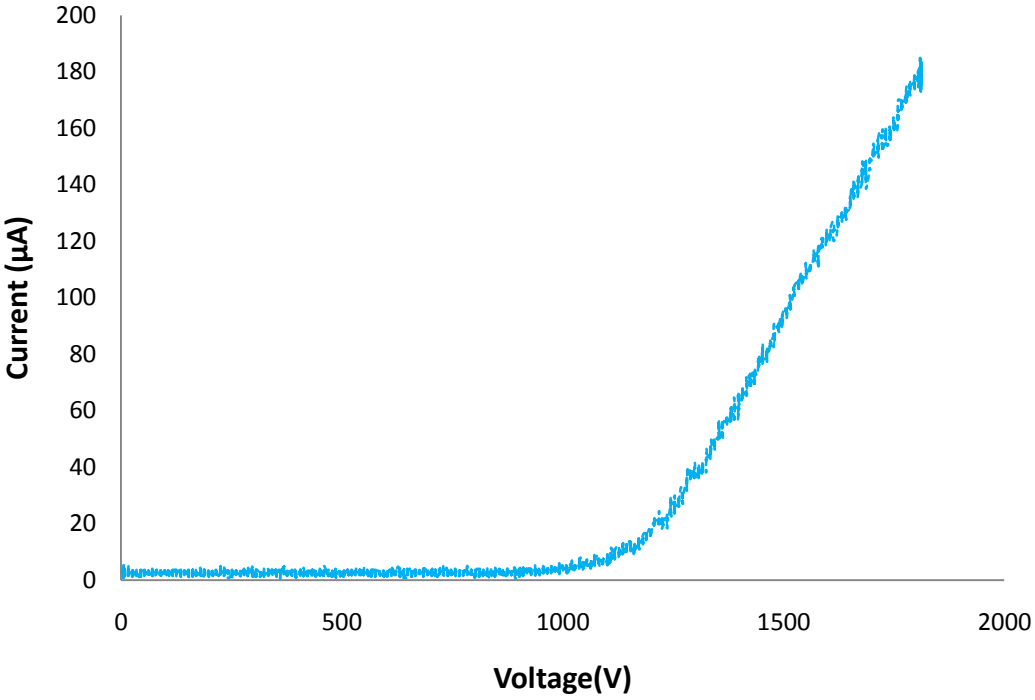

Figure 5-1: I/V Characteristic of Carbon Nanotubes Film

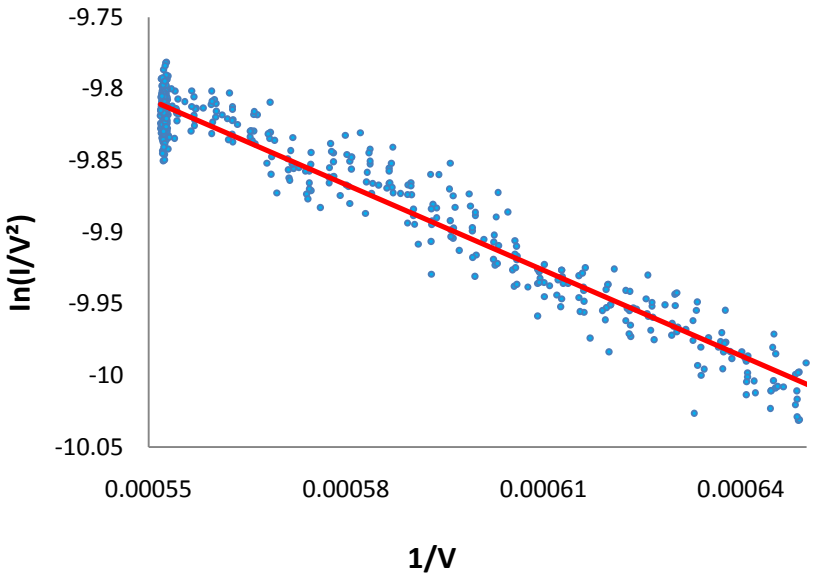

Figure 5-2: Fowler-Nordheim Plot

5.2 Long Term Stability

Figure 5-3 shows the plot of a long-term stability experiment. A constant voltage was applied to the anode, and the cathode was grounded. The experiment ran for more than 170 hours. In the first few hours, the current decreased very quickly. After 48 hours, the speed of decrease slowed and the curve became flat. The long-term current-time curve has a good agreement with a logarithm curve, as shown in the equation in Figure 5-3.

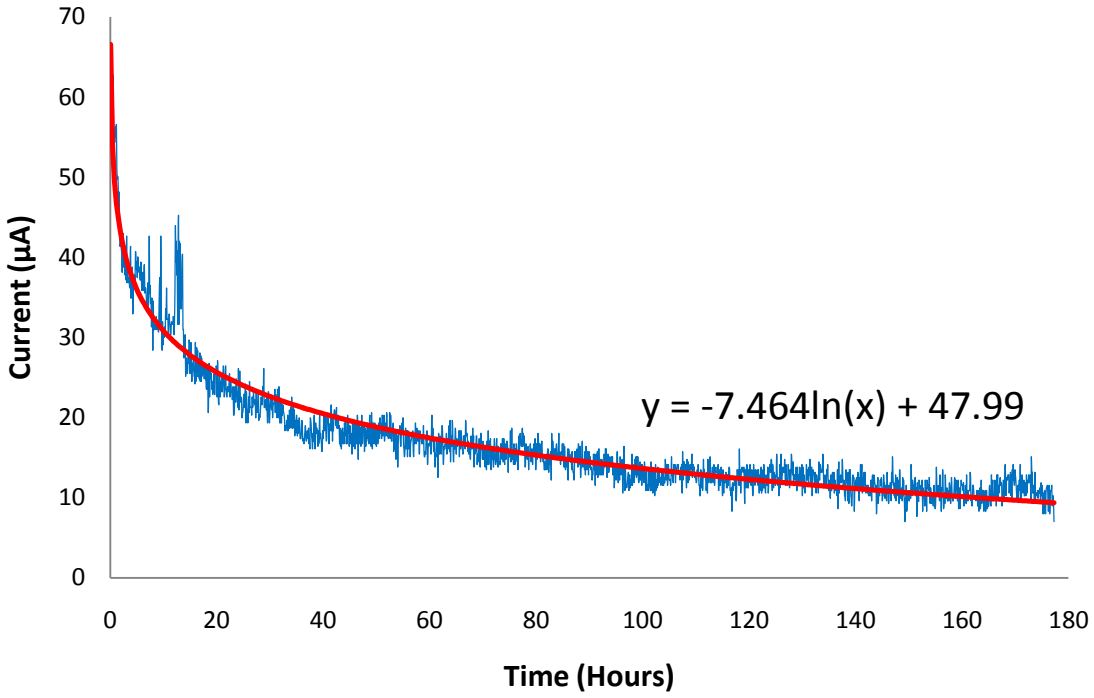

Figure 5-3: 170 Hours Stability of Emission Current

After this long-term experiment, visual inspection showed that some areas of the nanotube film had been destroyed. Figure 5-4 shows the SEM picture of a top view of the carbon

nanotube film after the experiment. In this picture, the dark areas are carbon nanotubes and the white areas are the copper substrate of the film where nanotubes were totally peeled off.

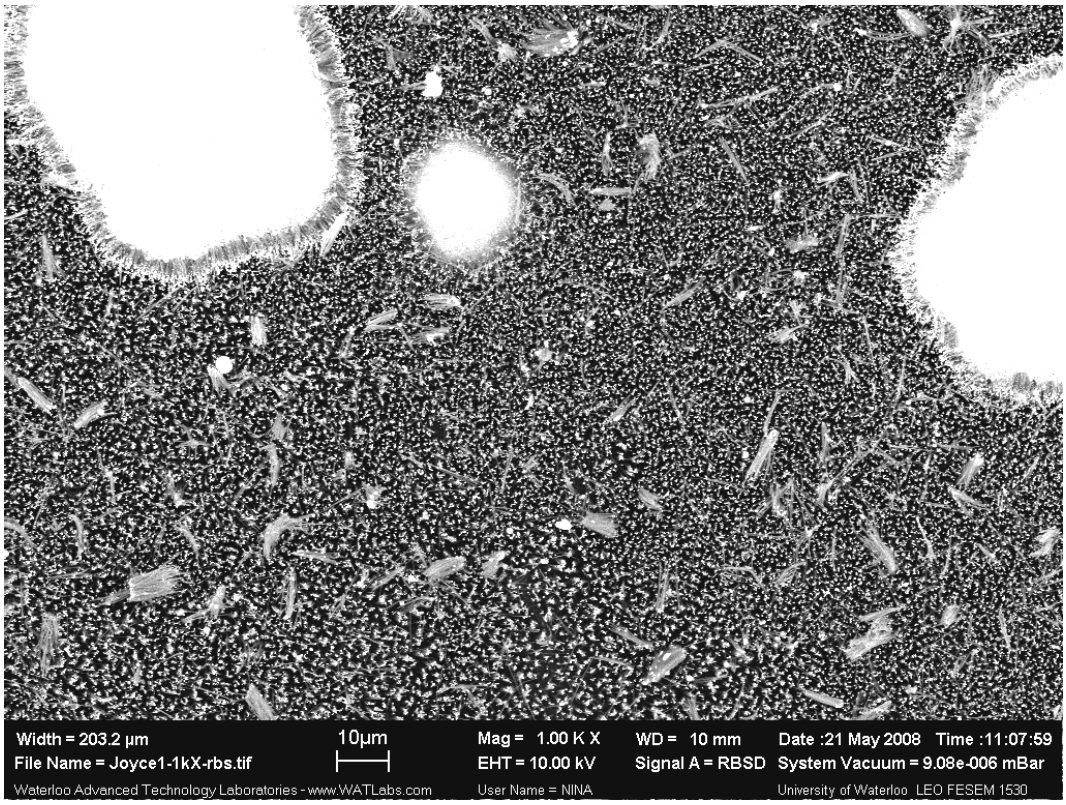

Figure 5-4: Carbon Nanotubes Film with Destroyed Area

It was reported that an eight thousand hour field emission was conducted [60], and the emission current had no obviously decrease. Due to the diversity of nanotubes, the stability of carbon nanotube film needs more investigation. According to the logarithm curve obtained in my experiments, the decline of the emission current will be slower and the current will be more stable.

5.3 Crosstalk Experiment

The crosstalk experiments were designed to study the possibility of fabricating a multi-pixel electron source. This experimental setup has a single nanotube film and four anodes. These anodes were mounted on an anode holder, so that the distances between them could be changed. The distances between anodes were 1.37 mm, 2.07 mm, 3.23 mm and 4.21 mm, separately. The anodes connected to either a high voltage or ground separately. Figure 5-5 and 5-6 show the current history of the anodes. In Figure 5-5, it can be clearly seen that as the current at the powered anode increases, the current collected at the grounded anode also increases. It is inferred from this figure that the current is leaking from one pixel to the neighboring pixel at a distance of 1.37 mm, and there is crosstalk. In the next experiment, the distance between neighboring anodes was increased to 3.23 mm. In Figure 5-6, it can be observed that as the distance between anodes was increased, the current collected at the grounded anode did not increase when the current at the powered anode increased. Instead, it oscillated between a maximum and a minimum, mainly due to noise. It can be concluded that the current at the grounded anode was independent of the current at the powered anode. Therefore, no crosstalk is observed when the neighboring anodes were 3.23 mm apart.

This crosstalk phenomenon indicates that there is a limitation of the smallest distance between the anodes in a multi-pixel X-ray sources design. Extra shielding between pixels is needed to prevent the electrons bombarding another anode. This shielding will increase the size of the X-ray tube.

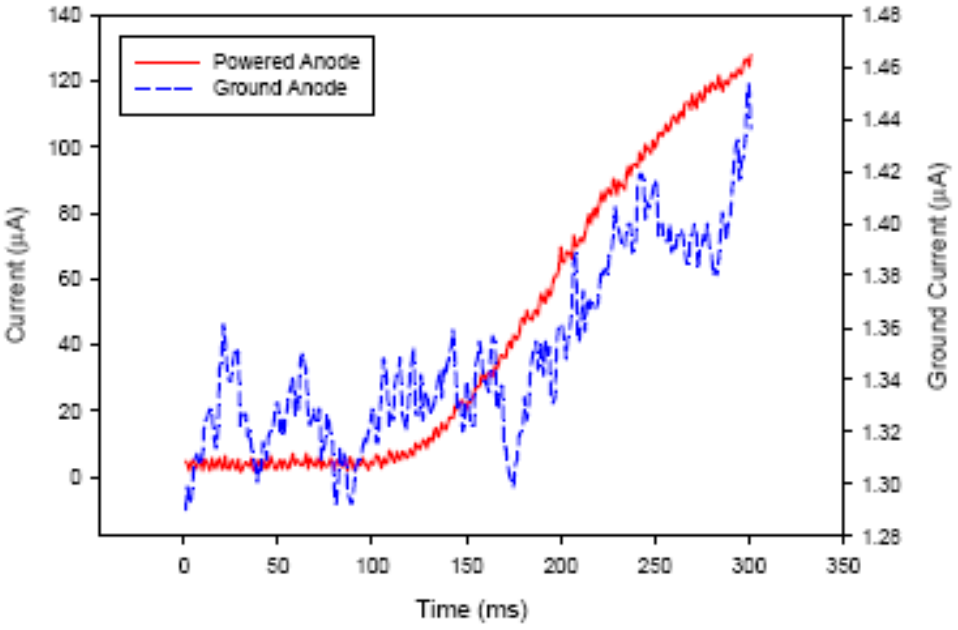

Figure 5-5: Crosstalk Current Between Anodes Close to Each Other

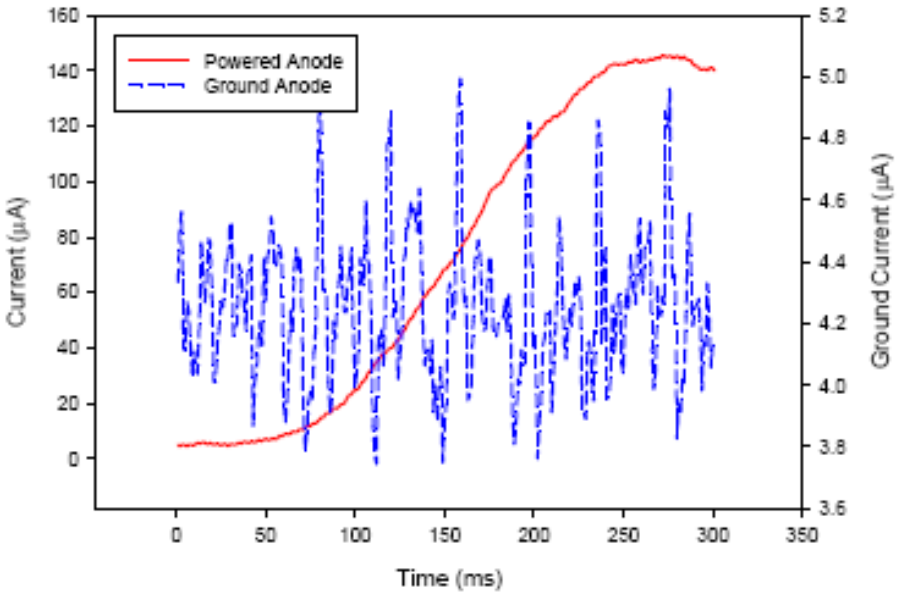

Figure 5-6: No Crosstalk Between Anodes Far Apart

5.4 Vacuum Breakdown

During the field emission experiments, vacuum breakdown was observed. The phenomenon showed the value of the vacuum pressure increasing by one or two orders and accompanied by a high spike current. In our data accusation system, the sample rate was 1 kHz, so the details of the current change could not be captured. In most cases, the spike current can make the power supply go into over-current protection mode. The output voltage dropped down rapidly, and as a consequence, the current decreased. Figure 5-7 shows the vacuum pressure and emission current change of a small breakdown. In this breakdown, the spike current is not very high; the power supply is in the normal working condition, the change of the vacuum pressure is relatively small.

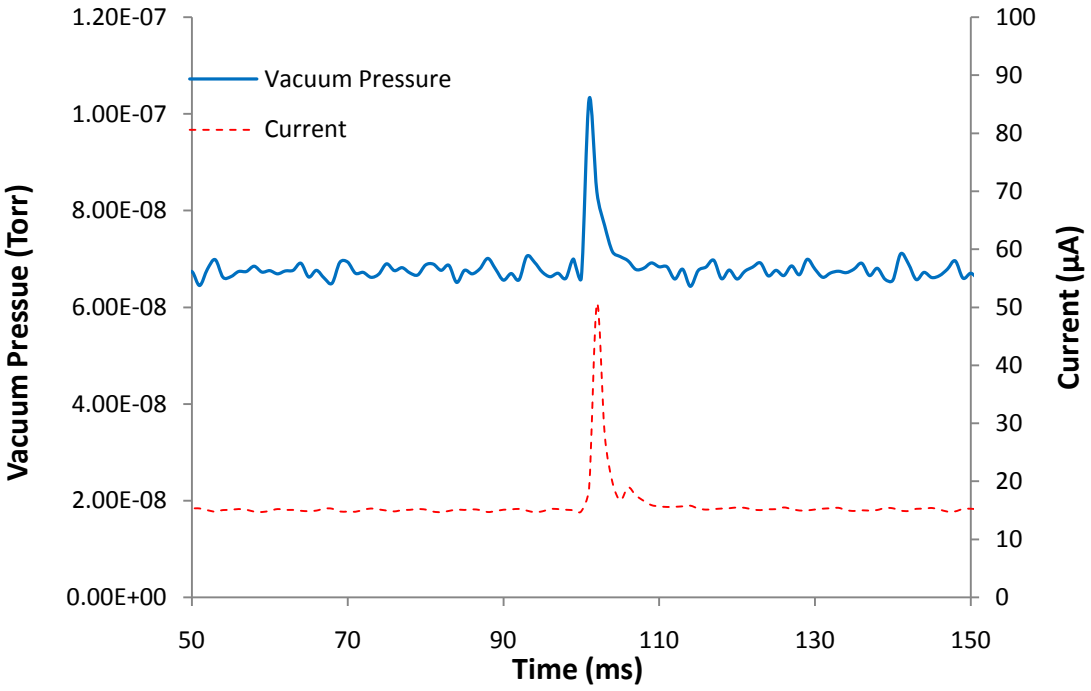

Figure 5-7: Vacuum Breakdown

Some researchers think that vacuum breakdown is caused by impurity or the amorphous carbon in the film, but others believe the spike current is a micro-arc in the gap. Based on the phenomena in our experiments, the explosive emission theory [28] is the best explanation of this current spike. When a high voltage is applied, the nanotubes, which are higher than others, have a much larger field enhancement factor. These nanotubes have a lower turn-on voltage and become the emission centers. The current is concentrated on these localized emission sites. Since the effective area of the emitter is so small, the current density becomes very high and a lot of heat is generated by Joule heat and Nottingham effect [10]. The temperature of the emitter cap can rise to over 3000 ℃. The high temperature and electrical field melt or pre-melt [62] the tips of the emitter, and some of the carbon molecules evaporate from the tip of the emitter. The evaporated molecules are ionized by the electrical field or the high temperature. These ions build up a discharge channel and cause the avalanche breakdown in the gap. After the micro-arc is generated, the tip of the nanotube, which is higher than others, is destroyed, and the nanotube is shortened. When the nanotube is not the longest in the area, a new emission center is established and a new micro-arc is generated. Figure 5-8 shows the stainless steel mesh in a triode structure experiment. It lasted for few hours at a relatively high current. Obviously, the metal has been melted by high temperature.

The process of avalanche in a vacuum lasts only few nano-seconds, and the diameter of carbon nanotubes is only few nanometers, so direct measurement of the temperature of a single nanotube and the quantity of the ions is not doable in my experiments. Although this

theory agrees well with the phenomena observed in the experiments, many details cannot be experimentally confirmed.

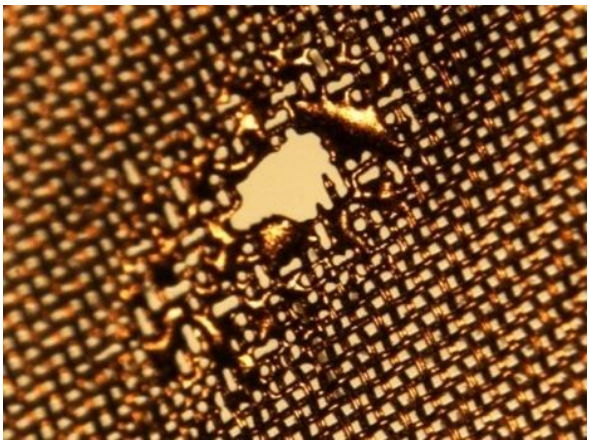

Figure 5-8: Stainless Steel Mesh was Melt

In the field emission experiments, when the strength of an electric field keeps constant and the gap is increased, the total number of breakdowns decreases. According to explosive emission theory, this reduction occurs because of the concentration of ions in the gap is not high enough to perform a discharge [28].

5.5 Degradation

Figure 5-9 shows the SEM image of the film after a short-time field emission experiment. The original state is shown in Figure 4-2. After field emission, the nanotubes were clustered and the orientation of the tubes changed from parallel to each other to random. This phenomenon may be caused by positive ion bombardment, but so far, there is no

experimental confirmation. In my experiments, this change did not affect the performance of the field emission much.

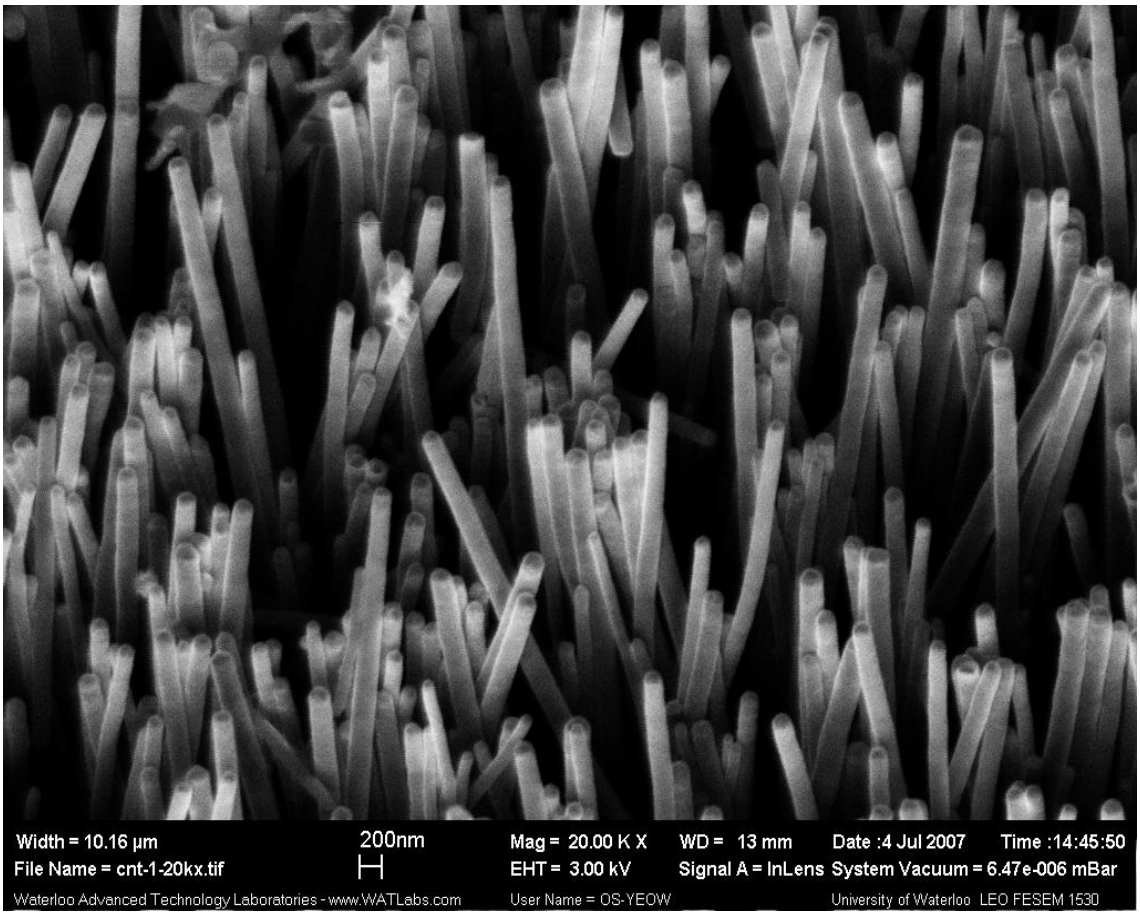

Figure 5-9: Nanotubes After Field Emission

Figure 5-10 shows the top view of the substrate where the carbon nanotubes were peeled off. This picture was taken after the 170-hour stability experiment. The substrate of the film is copper plate coated by a thick layer of chromium. In the picture, the left side shows some nanotubes, and the right side shows the substrate. The joints between nanotubes and substrate have bigger thermo and electrical resistivity than nanotubes, and the chemical bond is not as

strong as the bonds between carbon molecules. Thus, the temperature at these joint is higher than that in the tubes, and in this case, the carbon nanotubes can be peeled off easily [63, 64]. This peel off phenomena is also a possible reason for vacuum breakdown.

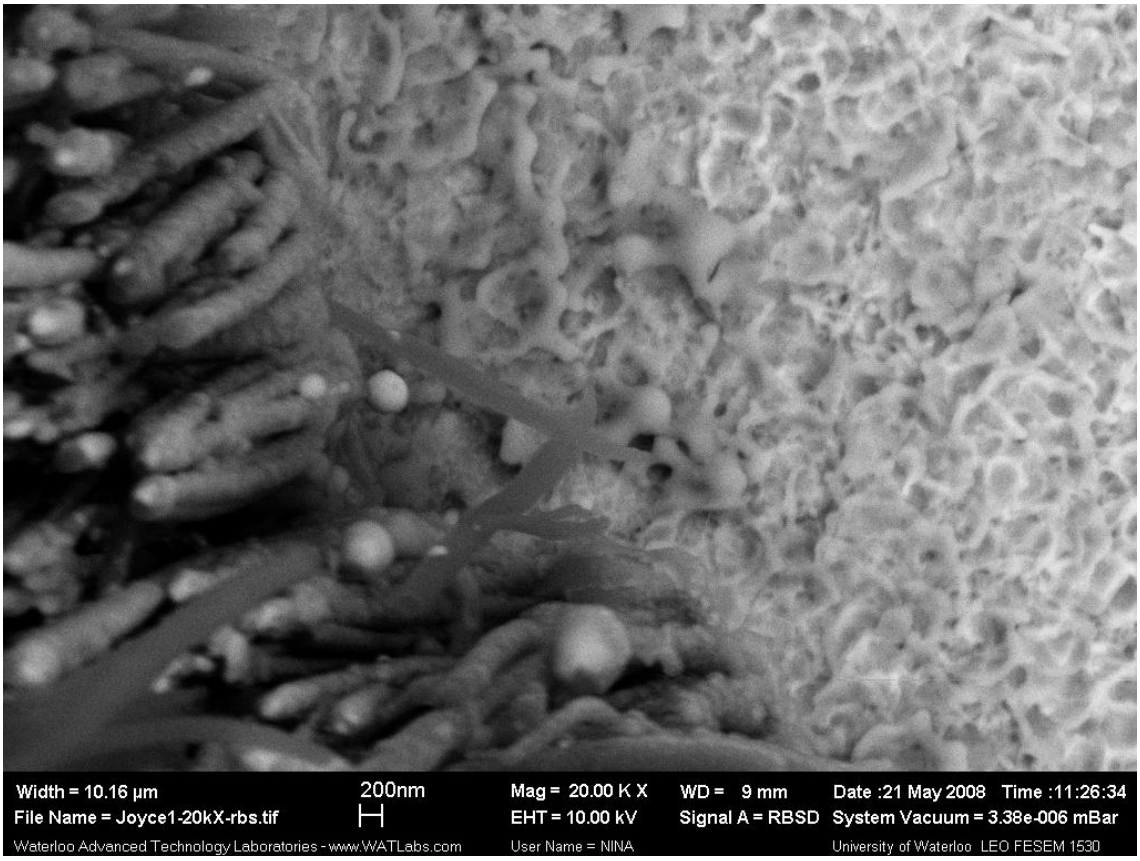

Figure 5-10: Substrate where the Nanotubes was Peeled Off

Figure 5-11 and 5-12 show dark spots on an anode after a long term stability experiment. The anode is made of copper plate. The dark spots correspond to the areas on the cathode where the nanotubes were peeled off. In the experiment, the electric field is controlled in a low current range to avoid vacuum breakdown. During the whole experiment, no big spike

current was observed. Under a microscope, the dark spots on anode look like small pits. At the center of each pit, there is a small gray-white protuberance. The EDX result shows that the dark spots are composed of carbon.

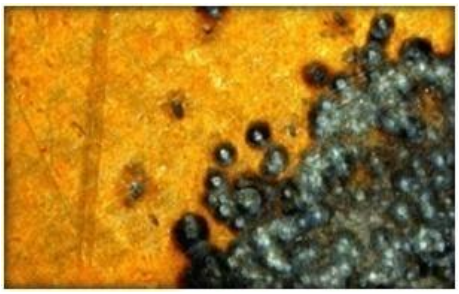

Figure 5-11: Dark Spots on Anode

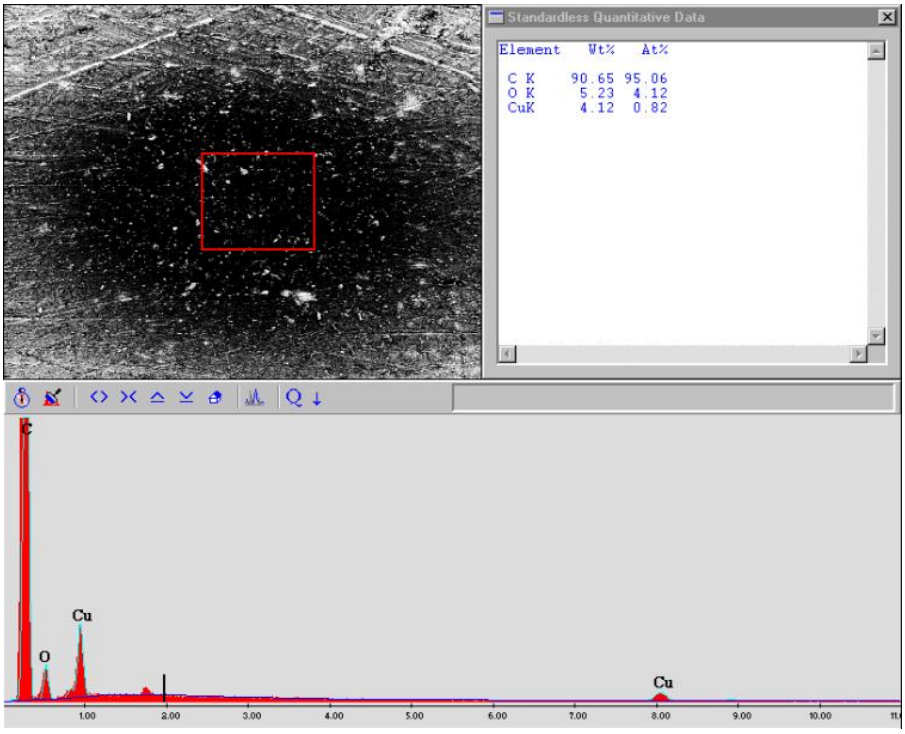

Figure 5-12: EDX result of Dark Spots

5.6 Other Experiments

Some other experiments were also conducted to test the performance of thin film emitters.

1. High voltages with different waveforms or frequency were applied to the diode setup. Since the cathode and the anode are metal plates with a very small gap, the capacitance is considerable. The equivalent circuit of the diode setup is a capacitor parallel to a diode. I-V characteristics of the emitter on different waveforms are the same up to a frequency of 10 Hz, and turn-on and turn-off delays of the emitter were not observed. But at a frequency higher than 10 Hz, the capacitance caused a significant change of the I-V characteristics. This capacitance will affect the maximum working frequency of the X-ray tube, so some further experiments are necessary to improve the frequency response of the carbon nanotube film emitter.
2. Nanotubes films with different substrates and different densities were tested.

   In these experiments, the affect of the substrate material was observed. Film on a copper substrate performs best, perhaps because copper has better thermo conductivity. In a field emission, a large amount of heat is generated by the Joule heating and Nottingham effect. Since carbon nanotubes have good thermo conductivity, radiation and convection can be neglected, and the heat generated at the tip of the nanotubes will be conducted to the substrate. A copper substrate can dissipate heat faster than a substrate made of stainless steel or quartz can, so nanotube film on a copper substrate performs better than that on other substrates.

In addition, nanotube films of different densities have been tested. Some of the samples used in these experiments had the highest density we could obtain from Nano-lab; others had an optimized density based on our calculation. Theoretically, the low density film should have performed better, but actually, the density of a sample made no significant difference. Furthermore, the long-term stability of a high-density film is much better than that of a low-density film

3. A triode configuration was used to test the structure of our X-ray tube. With a 25% opened mesh, up to 50% of the total emitted electrons passed through the gate and arrived the anode. Meshes of different density were tested, and the results show no significant difference
4. A phosphor screen was used as the anode of the diode setup in an experiment designed to determine the distribution of the emitting sites. During field emission, most areas of the screen were dark, except for some bright spots. The brightness and the position of these spots kept changing. The bright spots corresponded to the localized emission sites, and the changes corresponded to the degradation of the emitter. New nanotubes became the emitting center.

Chapter 6

Field Emission Optimization

6.1 Overview

In our experiments, carbon nanotubes have shown themselves to be good candidates for a field emission electron source. When compared to other electron emitters, however, carbon nanotubes apparently need more investigations when being used as a reliable high current electron source.

Because of the variety of carbon nanotube films, many factors affect their performance as emitters. Numerous experiments and simulations have been conducted by researchers interested in different aspects of the field of carbon nanotube emitters. There follows a brief discussion of important factors that should be considered in any attempt to improve the reliability and efficiency of carbon nanotube thin film emitters.

6.2 Type of Carbon Nanotubes

Nanotubes are categorized as single-wall nanotubes (SWNTs) and multi-wall nanotubes (MWNTs). Most single-wall nanotubes have a diameter of close to only a few nanometers. Single-wall nanotubes are a very important variant of carbon nanotubes because they exhibit important electric properties that are not shared by the multi-wall carbon nanotube variants [65]. Carbon nanotubes are also categorized based on whether their type of cap is closed, opened, or catalyst-topped. Bonard et al. tested the performances of four types of carbon

nanotube emitters [66]. The turn-on field and threshold field of these nanotube films were compared and their characteristic I-V curves are shown in Figure 6-1 [51]. Theoretically, since the single-wall nanotubes have the smallest diameter, they should have the best field emission performance, but in these experiments, the closed multi-wall carbon nanotubes have the lowest turn-on field and threshold field. The researchers believe that this phenomenon occurs because single-wall nanotubes are easy to bundle in ropes.

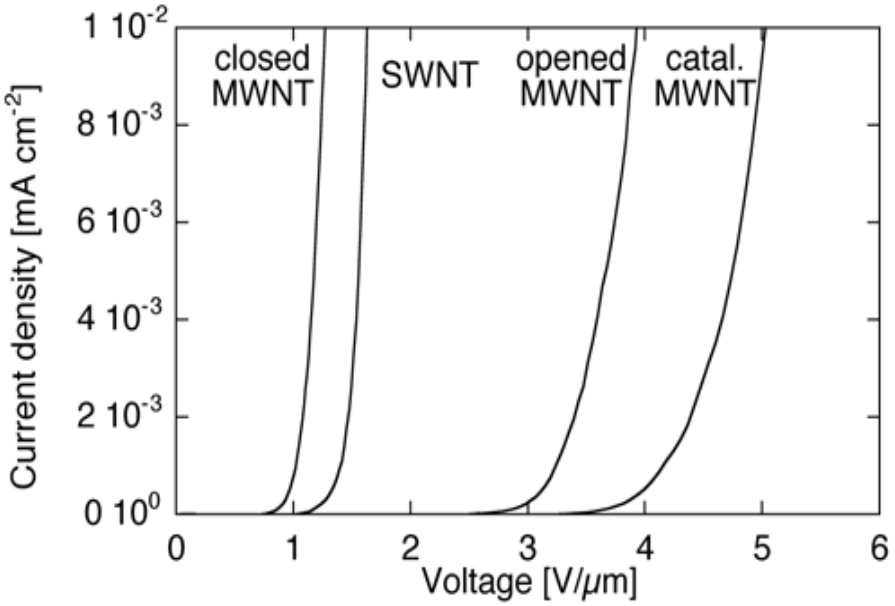

Figure 6-1: Emission Performances of Different Nanotubes

In my experiments, the films were composed of aligned closed multi-wall nanotubes with a diameter of about 100 nm. Compared to the most common nanotubes, the sidewalls of these nanotubes are relatively thick, so the field enhancement factor is low. In the following experiments, other types of nanotubes are tested to identify the best type for our application.

6.3 Density of Carbon Nanotubes

In order to determine the best density for aligned nanotubes used in field emission testing, electrostatic calculations were performed on the field penetration between parallel standing tubes. Figure 6-2 shows a 2-D simulation result of the strength of the electrostatic field and the equipotential lines for tubes with different distance. In this calculation, the aspect ratio of the nanotubes is set to 1000:1; the distance between tubes is 0.25, 0.5,1 and 1.5 times the height of the tubes. The equipotential lines and strength of the field are significantly affected as the inter-tube distance is decreased.

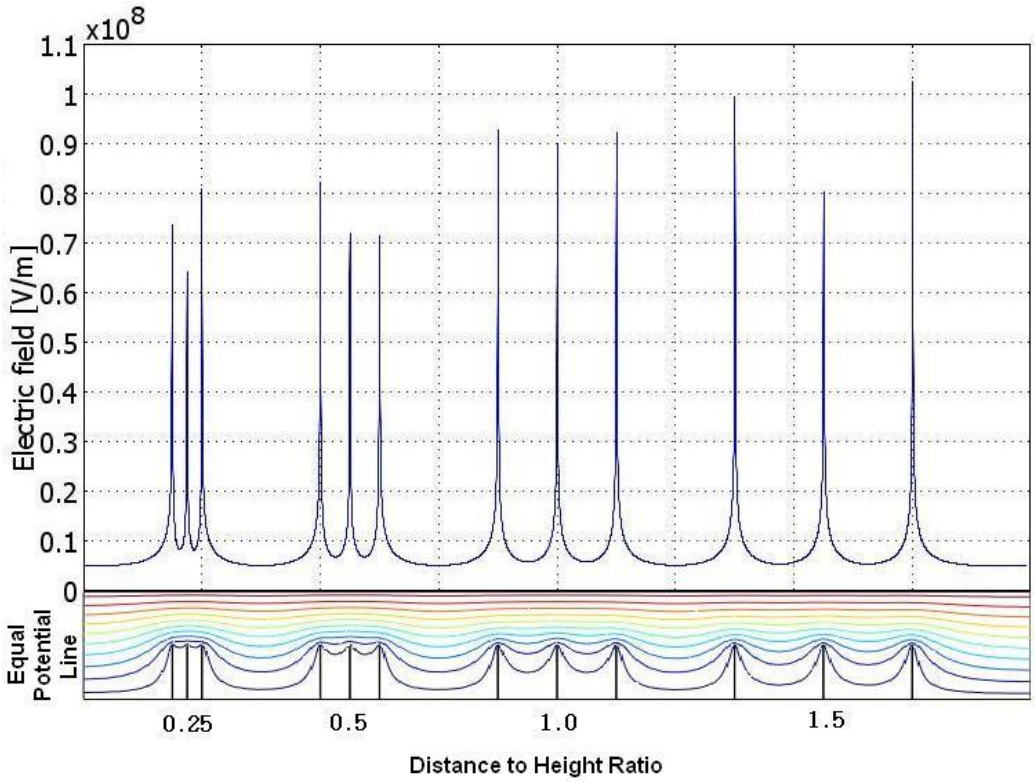

Figure 6-2: Simulation Result of Different Densities

The screening effect between nanotubes decreased the field strength and thus decreased the field enhancement factor, β, but a large distance will decrease the density of emitters, and thus decrease the total number of emitters. A field emission experiment performed by Nilsson et al [67] proved that medium-density nanotube film has better emission performance than low- and high-density films.

Some calculations show that theoretically, the best height vs. distance ratio for the aligned nanotube film is about 1:1. In our experiments, no major difference was observed because the nanotubes in a film do not have exactly equal length; the longer tubes are not affected by the screen effect of neighboring short ones. Moreover, higher total emitter numbers can make these films have a longer lifetime. More experiments are needed to find out the best density for nanotubes in a thin film emitter.

6.4 Diameter of Carbon Nanotubes

The diameter of carbon nanotubes affects field emission in two ways. Thinner tubes have a higher field enhancement factor. That is, the turn-on filed of thin tubes is lower than the thick ones. On the other hand, the relationship between Joule heat and diameter is $T_{Joule} \propto 1/r^4$. The thinner tube needs much lower current to achieve the melting point of the tubes or the substrate than thicker tubes need. Since carbon nanotubes have very a high melting point and good thermo conductivity, and the weakest point of the films is the joint between the tube and substrate, thinner tubes should therefore be easier to peel off from the substrates. Some researchers have reported a method for fabricating multistage nanotubes [68], which consist

of multi-wall carbon nanotubes grown on a metal substrate and a single-wall carbon nanotube grown on each of the multi-wall carbon nanotubes. Since these tubes have the advantages of both single-wall and multi-wall nanotubes, they should have perform better than other nanotubes. We will try to fabricate these kinds of nanotubes and test their field emission performance.

6.5 Atomic Structure of Emitter Tip

In metal emitter studies, the cathode's surface is comprised of different crystallographic planes with different work functions and local radii of curvature. By the Fowler-Nordheim equation, these distinctions in geometry and work functions result in a variation in emission current density over the apex of the emitter tip. Typically, the <110> direction has a relatively high work function in additional to creating a relatively large and flat crystal plane on the tip, resulting in the emission current density along the tip axis being small. In electron optical applications, the most intense electron emission directed along the optical axis is preferred. Thus, orientations of <111>, <100> and <310> are always chosen [10].

In aligned nanotube film, emitting sites are the tips, and in random films, emitting sites are at both the tips and defects. In metal emitter studies, a low work function metal is used to coat the emitter and produce an improved metal emitter [69]. We will employ this method in future experiments, i.e., coating a thin layer of metal on the surface of carbon nanotube emitters to improve their emission properties.

Chapter 7

Summary and Future Work

7.1 Summary

The goal of this research is to design stable high performance electron sources for a multi-pixel X-ray array. Many experiments were conducted to study the field emission properties of carbon nanotube film. Certain other research groups have demonstrated their prototype carbon nanotube-based X-ray tubes. These studies and my experiments show the feasibility of using carbon nanotubes as a field emission electron source. Although field emission cathode design is now possible, the stability and lifetime of carbon nanotube-based electron sources are not as good as those for conventional designs.

Conventional field emission theories have studied metal and semiconductor emitters. The unique properties of carbon nanotubes mean that many results of field emission experiments are inexplicable by those theories. Thus, the mechanism of carbon nanotube field emission is not quite clear, and further studies are required.

Furthermore, it is reported that when compared to traditional thermo emission X-ray tubes, the carbon nanotube based cold cathode X-ray tube has some inimitable characteristics. To date, in vivo experiments have not been conducted. It is still unknown how the new design will affect the future of medical diagnosis.

In conclusion, although carbon nanotube field emission has been studied widely, both carbon nanotube-based field emitters and medical devices using them are still in the stage of laboratory research. We have a lot of work to do before this technology can be commercially produced and used to benefit patients.

7.2 Future Work

In previous work, the diode and triode configuration have been tested and the carbon nanotube film displays good field emission properties. Based on the results of these experiments, the following investigations are planned.

1. Improve the performance

   Carbon nanotube-based X-ray tubes are still in the laboratory study stage and many parameters may affect the performance and lifetime of the emitters and X-ray tubes. In this thesis, some possible factors have been discussed. Additional experiments, e.g., testing the carbon nanotubes with different density, height, orientation, and cap shape and substrate, will be conducted to identify the ways to improve performance.

   Finding other methods to excite electron emission, but which greatly decrease emission and control voltages is also central to my planned research.

2. Focus the electron beam

   One important parameter of the micro-CT scanner is the size of its focal spot. A unique advantage of field emission is the very small electron energy spread; the emission area is thus small and the beam is highly coherent. This property of field

emitters makes focusing the electron beam on a small spot easy. Currently, micrometer scale focal spots have been achieved by field emission X-ray tubes.

In my previous studies, different types of electronic lens have been designed and simulated. Each type of electronic lens has its own advantages. The electronic lens will be fabricated and tested in the following months.

3. Address multiple pixels

One of the bottlenecks of conventional CT scanners is X-ray source. Even with a very high rotating speed, the single beam CT scanner still cannot be used in cardiac imaging. The biggest advantage of a multi X-ray source CT scanner is not just that it has no moving parts, but also that it scans at high speeds. Multiple modulated X-ray beams can be emitted synchronously, and the demodulate algorithm can reconstruct 3D images rapidly [70]. This feature can reduce scanning time significantly.

Regular addressing methods can light up one pixel at a time. To achieve multiple beam scans, a complex multi-pixel addressing system is needed. On the other hand, the design of the addressing circuit relies on the method of controlling pixels. To allow switching of the high voltage applied to the gate electrodes at high speed, in the future, special circuits will be designed and tested.

Bibliography

[1] Sinha, N., Mahapatra, D.R., Yeow, J.T.W., "Modeling the Field Emission Current Fluctuation in Carbon Nanotube Thin Films," 2007,

[2] Wood, R.W., "A New Form of Cathode Discharge and the Production of X-Rays, together with Some Notes on Diffraction. Preliminary Communication," *Phys.Rev.(Series I)*, Vol. 5, No. 1, 1897, pp. 1-10.

[3] Fowler, R.H., and Nordheim, L., "Electron Emission in Intense Electric Fields," *Proceedings of the Royal Society of London.Series A, Containing Papers of a Mathematical and Physical Character*, Vol. 119, No. 781, 1928, pp. 173-181.

[4] Iijima, S.1., "Helical microtubules of graphitic carbon," *Nature*, Vol. 354, No. 6348, 1991, pp. 56-8.

[5] Rinzler, A.G., Hafner, J.H., Nikolaev, P., "Unraveling Nanotubes: Field Emission from an Atomic Wire," *Science*, Vol. 269, No. 5230, 1995, pp. 1550-1553.

[6] Sinha, N., "Characterization of Carbon Nanotube Based Thin Film Field Emitter," 2008,

[7] Purdie, T.G., Bissonnette, J., Franks, K., "Cone-Beam Computed Tomography for On-Line Image Guidance of Lung Stereotactic Radiotherapy: Localization, Verification, and Intrafraction Tumor Position," *International Journal of Radiation Oncology Biology Physics*, Vol. 68, No. 1, 2007, pp. 243-252.

[8] White, E.A., Cho, J., Vallis, K.A., "Cone Beam Computed Tomography Guidance for Setup of Patients Receiving Accelerated Partial Breast Irradiation," *International Journal of Radiation Oncology Biology Physics*, Vol. 68, No. 2, 2007, pp. 547-554.

[9] Memphis Radiological, P., "Radiation therapy,"

[10] Fursey, G., "Field emission in vacuum microelectronics," *Microdevices*, Kluwer Academic/Plenum Publishers, New York, 2005, pp. xv, 205 p.

[11] Henderson, J.E., and Dahlstrom, R.K., "The Energy Distribution in Field Emission," *Phys.Rev.*, Vol. 55, No. 5, 1939, pp. 473-481.

[12] Dolan, W.W., Dyke, W.P., and Trolan, J.K., "The Field Emission Initiated Vacuum Arc. II. The Resistively Heated Emitter," *Phys.Rev.*, Vol. 91, No. 5, 1953, pp. 1054-1057.

[13] Dyke, W.P., and Trolan, J.K., "Field Emission: Large Current Densities, Space Charge, and the Vacuum Arc," *Phys.Rev.*, Vol. 89, No. 4, 1953, pp. 799-808.

[14] Charbonnier, F.M., Barbour, J.P., Brewster, J.L., "Intense, Nanosecond Electron Beams," *Proceedings of the 2nd IEEE Particle Accelerator Conference*, Vol. NS-14, 1967, pp. 789.

[15] Fursey, G.N., "Field Emission and Vacuum Breakdown," *Electrical Insulation, IEEE Transactions on [See also Dielectrics and Electrical Insulation, IEEE Transactions on]*, Vol. EI-20, No. 4, 1985, pp. 659-670.

[16] Crewe, A.V., Eggenberger, D.N., Wall, J., "Electron Gun Using a Field Emission Source," *Review of Scientific Instruments*, Vol. 39, No. 4, 1968, pp. 576-583.

[17] Spindt, C.A., Holland, C.E., Brodie, I., "Field-emitter arrays to vacuum fluorescent display," *Electron Devices, IEEE Transactions on,* Vol. 36, No. 1; essentially a miniature cathode-ray tube (CRT), the device has the potential to produce brightness similar to those on a CRT in a panel that is 3.3 in square (8.4 cm) in area and 0.15 in (4 mm) thick, 1989, pp. 225-228.
[18] Bell, A.E., and Swanson, L.W., "Total energy distributions of field-emitted electrons at high current density," *Physical Review B (Condensed Matter),* Vol. 19, No. 7, 1979, pp. 3353-64.
[19] Fowler, R.H., and Nordheim, L., "Electron Emission in Intense Electric Fields," *Proceedings of the Royal Society of London.Series A, Containing Papers of a Mathematical and Physical Character,* Vol. 119, No. 781, 1928, pp. 173-181.
[20] Murphy, E.L., and Good, R.H., "Thermionic Emission, Field Emission, and the Transition Region," *Phys.Rev.,* Vol. 102, No. 6, 1956, pp. 1464-1473.
[21] Gadzuk, J.W.1., and Plummer, E.W.1., "Field emission energy distribution (FEED)," *Reviews of Modern Physics,* Vol. 45, No. 3, 1973, pp. 487-548.
[22] Rodnevich, B.B., "Energy spectrum of field emission," *Vacuum Microelectronics Conference, 1996. IVMC'96., 9th International,* 1996, pp. 77-80.
[23] Charbonnier, F.M., Strayer, R.W., Swanson, L.W., "Nottingham Effect in Field and $T-F$ Emission: Heating and Cooling Domains, and Inversion Temperature," *Physical Review Letters,* Vol. 13, No. 13, 1964, pp. 397-401.
[24] Glazanov, D.V., Baskin, L.M., and Fursei, G.N., "Kinetics of the pulsed heating of field-emission cathode points with real geometry by a high-density emission current," *Soviet Physics - Technical Physics,* Vol. 34, No. 5, 1989, pp. 534-9.
[25] Baskin, L.M., Glazanov, D.V., and Fursei, G.N., "Influence of thermoelastic stresses on the destruction of field-emission cathode points and the transition to explosive emission," *Soviet Physics - Technical Physics,* Vol. 34, No. 5, 1989, pp. 579-80.
[26] Bugaev, S.P., Litvinov, E.A., Mesyats, G.A., "Explosive emission of electrons," *Uspekhi Fizicheskii Nauk,* Vol. 115, No. 1, 1975, pp. 101-20.
[27] Su, Y., Chen, W., Wang, F., "Cathode spots on the surface of nanostructured W alloys," *Materials Letters,* Vol. 59, No. 8-9, 2005, pp. 1046-1049.
[28] Mesyats, G.A., "Explosive Electron Emission," URO-Press, Ekaterinburg, 1998, pp. 248.
[29] Mesyats, G.A., "Cathode Phenomena in a Vacuum Discharge: The Breakdown, the Spark and the Arc," Nauka Publishers, MOSCOW, 2000,
[30] Alpert, D., Lee, D.A., Lyman, E.M., "Initiation of Electrical Breakdown in Ultrahigh Vacuum," *Journal of Vacuum Science and Technology,* Vol. 1, No. 2, 1964, pp. 35-50.
[31] Chatterton, P.A., "A theoretical study of field emission initiated vacuum breakdown," *Proceedings of the Physical Society,* Vol. 88, No. 1, 1966, pp. 231-245.
[32] Iijima, S., and Ichihashi, T., "Single-shell carbon nanotubes of 1-nm diameter," *Nature,* Vol. 363, No. 6430, 1993, pp. 603.
[33] Anantram, M.P., and L\'{e}onard, F., "Physics of carbon nanotube electronic devices," *Reports on Progress in Physics,* Vol. 69, No. 3, 2006, pp. 507-561.

[34] Tomanek, D., "Nanotube Site,"
[35] Klinke, C., and Noury, O., "Nanotube Basics,"
[36] Charlier, J., Blase, X., and Roche, S., "Electronic and transport properties of nanotubes," *Reviews of Modern Physics,* Vol. 79, No. 2, 2007, pp. 677.
[37] Yan, K.Y., Xue, Q.Z., Zheng, Q.B., "The interface effect of the effective electrical conductivity of carbon nanotube composites," *Nanotechnology,* Vol. 18, No. 25, 2007, pp. 255705 (6pp).
[38] Cai, J., Bie, R.F., Tan, X.M., "Application of the tight-binding method to the elastic modulus of C60 and carbon nanotube," *Physica B: Condensed Matter,* Vol. 344, No. 1-4, 2004, pp. 99-102.
[39] Kim, P., Shi, L., Majumdar, A., "Thermal Transport Measurements of Individual Multiwalled Nanotubes," *Physical Review Letters,* Vol. 87, No. 21, 2001, pp. 215502.
[40] Dobrokhotov, V., and Berven, C.A., "Electronic transport properties of metallic CNTs in an axial magnetic field at nonzero temperatures: A model of an ultra-small digital magnetometer," *Physica E: Low-Dimensional Systems and Nanostructures,* Vol. 31, No. 2, 2006, pp. 111-116.
[41] Saito, R., Fujita, M., Dresselhaus, G., "Electronic structure of chiral graphene tubules," *Applied Physics Letters,* Vol. 60, No. 18, 1992, pp. 2204-2206.
[42] Charlier, J.-., "Defects in Carbon Nanotubes," *Accounts of Chemical Research,* Vol. 35, No. 12, 2002, pp. 1063-1069.
[43] Agrawal, S., Raghuveer, M.S., Li, H., "Defect-induced electrical conductivity increase in individual multiwalled carbon nanotubes," *Applied Physics Letters,* Vol. 90, No. 19, 2007, pp. 193104.
[44] Haibo Fan, Kai Zhang, and Yuen, M.M.F., "Effect of defects on thermal performance of carbon nanotube investigated by molecular dynamics simulation," *Electronic Materials and Packaging, 2006. EMAP 2006. International Conference on,* 2006, pp. 1-4.
[45] de Jonge, N., "Brightness of carbon nanotube electron sources," *Journal of Applied Physics,* Vol. 95, No. 2, 2004, pp. 673-681.
[46] Jang, H.-., Kang, S.-., Nahm, S.-., "Field emission characteristics of an individual carbon nanotube inside a field emission-scanning electron microscope," *Vacuum,* Vol. 81, No. 4, 2006, pp. 422-426.
[47] Fujieda, T., Hidaka, K., Hayashibara, M., "Direct observation of field emission sites in a single multiwalled carbon nanotube by Lorenz microscopy," *Japanese Journal of Applied Physics, Part 1 (Regular Papers, Short Notes & Review Papers),* Vol. 44, No. 4, 2005, pp. 1661-4.
[48] Saito, Y., Hata, K., and Murata, T., "Field emission patterns originating from pentagons at the tip of a carbon nanotube," *Japanese Journal of Applied Physics, Part 2: Letters,* Vol. 39, No. 4, 2000, pp. 271-272.
[49] Charlier, J.-., and Issi, J.-., "Electrical conductivity of novel forms of carbon," *Journal of Physics and Chemistry of Solids,* Vol. 57, No. 6-8, 1996, pp. 957-965.

[50] Endo, M., Takeuchi, K., Kobori, K., "Pyrolytic carbon nanotubes from vapor-grown carbon fibers," *Carbon,* Vol. 33, No. 7, 1995, pp. 873-881.
[51] Bonard, J.M., Salvetat, J.P., Stockli, T., "Field emission from carbon nanotubes: perspectives for applications and clues to the emission mechanism," *Applied Physics A (Materials Science Processing),* Vol. A69, No. 3, 1999, pp. 245-54.
[52] Oshima, C., Matsuda, K., Kona, T., "Electron emission sites on carbon nanotubes and the energy spectra," *Japanese Journal of Applied Physics, Part 2: Letters,* Vol. 40, No. 11, 2001, pp. 1257-1259.
[53] Liu, P., Sun, Q., Zhu, F., "Measuring the work function of carbon nanotubes with thermionic method," *Nano Letters,* Vol. 8, No. 2, 2008, pp. 647-651.
[54] Young Hee Lee, Seong Chu Lim, Hee Jin Jeong, "Extracting independently the work function and field enhancement factor from thermal-field emission of multi-walled carbon nanotube tips," *Carbon,* Vol. 43, No. 13, 2005, pp. 2801-7.
[55] Shiraishi, M., and Ata, M., "Work function of carbon nanotubes," *Symposium,* Mater. Res. Soc, Boston, MA, USA, 2001, pp. 4-4.
[56] Suzuki, S., Bower, C., Watanabe, Y., "Work functions and valence band states of pristine and Cs-intercalated single-walled carbon nanotube bundles," *Applied Physics Letters,* Vol. 76, No. 26, 2000, pp. 4007-4009.
[57] Itoh, S., "Current Status of the Spindt-type Field Emitter," *Discharges and Electrical Insulation in Vacuum, 2006. ISDEIV '06. International Symposium on,* Vol. 2, 2006, pp. 875-876.
[58] Zhu, W., Kochanski, G.P., and Jin, S., "Low-Field Electron Emission from Undoped Nanostructured Diamond," *Science,* Vol. 282, No. 5393, 1998, pp. 1471-1473.
[59] NASA, "Outgassing Data for Selecting Spacecraft Materials," 2008,
[60] Saito, Y., and Uemura, S., "Field emission from carbon nanotubes and its application to electron sources," *Carbon,* Vol. 38, No. 2, 2000, pp. 169-182.
[61] Sinha, N., Yeow, J.T.W., and Jaffray, D.A., "Experimental Investigation of the Crosstalk Phenomenon and Current Stability in a Carbon Nanotube Array," Proc. 7th IEEE International Conference on Nanotechnology, Hong Kong, August 02-05, 2007,
[62] Zhang, K., Stocks, G.M., and Zhong, J., "Melting and premelting of carbon nanotubes," *Nanotechnology,* Vol. 18, No. 28, 2007, pp. 285703 (5pp).
[63] Huang, N.Y., She, J.C., Chen, J., "Mechanism responsible for initiating carbon nanotube vacuum breakdown," *Physical Review Letters,* Vol. 93, No. 7, 2004, pp. 075501-1.
[64] Chen, J., She, J.C., Xu, N.S., "Vacuum breakdown of carbon-nanotube field emitters on a silicon tip," *Applied Physics Letters,* Vol. 83, No. 13, 2003, pp. 2671-2673.
[65] Dekker, C., "Carbon nanotubes as molecular quantum wires," *Physics Today,* Vol. 52, No. 5, 1999, pp. 22-8.
[66] Bonard, J.-., Kind, H., Stockli, T., "Field emission from carbon nanotubes: The first five years," *Solid-State Electronics,* Vol. 45, No. 6, 2001, pp. 893-914.
[67] Nilsson, L., Groening, O., Emmenegger, C., "Scanning field emission from patterned carbon nanotube films," *Applied Physics Letters,* Vol. 76, No. 15, 2000, pp. 2071-2073.

[68] Seelaboyina, R., Boddepalli, S., Noh, K., "Enhanced field emission from aligned multistage carbon nanotube emitter arrays," *Nanotechnology,* Vol. 19, No. 6, 2008, pp. 065605.
[69] Zhang, J., Yang, C., Wang, Y., "Improvement of the field emission of carbon nanotubes by hafnium coating and annealing," *Nanotechnology,* Vol. 17, No. 1, 2006, pp. 257-260.
[70] Lalush, D.S., Quan, E., Rajaram, R., "Tomosynthesis reconstruction from multi-beam X-ray sources," *2006 3rd IEEE International Symposium on Biomedical Imaging: From Nano to Macro,* Vol. 2006, Institute of Electrical and Electronics Engineers Computer Society, Piscataway, NJ 08855-1331, United States, Arlington, VA, United States, 2006, pp. 1180-1183.